Changes in the Low-Level Kinematic and Thermodynamic Structure of Hurricane Alicia (1983) at Landfall

MARK D. POWELL

NOAA/Atlantic Oceanographic and Meteorological Laboratory, Miami, Florida 33149

(Manuscript received 2 January 1986, in final form 7 July 1986)

ABSTRACT

Aircraft, land station, and buoy data were composited with respect to the center of Hurricane Alicia (1983) for three 8-h periods corresponding to prelandfall in the open Gulf of Mexico, landfall in the Galveston area, and postlandfall in the vicinity of Houston.

Comparison of the wind analyses before, during, and after landfall emphasizes the land–sea frictional asymmetry at landfall. In addition, other asymmetries in the surface wind field and differences between the flight-level and the surface wind fields are revealed. The asymmetric structure of the surface wind field may be interpreted as having resulted from the combined effects of land–sea roughness differences, background environmental flow, and storm translation. The land–sea frictional difference acted to oppose the mean vortex flow over land and reinforce it over water. The southwest background environmental flow acted nearly parallel to the coastline, producing surface inflow on the left side and outflow on the right side, while the effect of the storm translation increased winds on the right and decreased winds on the left. At landfall, the analysis revealed a broad region of high wind speeds and a mesoscale divergence–convergence couplet along the outer rainband axis just offshore on the northeast (right) side of the storm. The outer rainband axis acted as an obstruction to the surface flow, separating the warmer central core of the storm from the environment through which the storm moved. In contrast to recent numerical model studies, surface convergence was also noted on the left side of the storm just offshore, despite outflow at flight level.

Analyses of temperature, dewpoint, and equivalent potential temperature indicate that loss of the oceanic heat and moisture source, combined with advection of drier air on the landward side of the storm, was responsible for cooling and drying of the inflowing boundary layer air. Upon introduction of this air into the core convection and vertical ascent, a decrease in the release of latent heat could then lead to cooling in the middle levels of the storm and a subsequent increase in the central sea-level pressure.

1. Introduction

A hurricane undergoes major changes when it moves from an oceanic to a land environment. Landfall drastically reduces the supply of heat and moisture believed to be necessary for maintenance of the storm (Miller, 1964; Rosenthal, 1971). Frictional and thermal effects over land may influence the future motion of the storm (Moss and Jones, 1978) and produce features in the mesoscale wind and precipitation structure that are related to the areas of heaviest damage (Powell, 1982; Parish et al., 1982). The physical mechanisms associated with the weakening of the hurricane at landfall are of special interest to forecasters who must interpret aircraft reconnaissance and coastal observations before and during landfall for warning purposes. Such information is also useful to engineers and planners for the design of hurricane-resistant structures.

Since the advent of aircraft reconnaissance of tropical storms and the National Hurricane Research Project in 1956, much has been learned about the synoptic, vortex, and mesoscale structure and dynamics of hurricanes. Recently, with the advent of the NOAA WP-3D instrumented research aircraft (Merceret and Davis, 1981), knowledge of mesoscale (e.g., Barnes et al., 1983; Jorgensen, 1984; Marks and Houze, 1984) and vortex-scale (e.g., Shapiro and Willoughby, 1982; Willoughby et al., 1984) structure and dynamics has improved dramatically. However, the bulk of our knowledge is based upon storm behavior over open water. Since overflying land is too hazardous in landfalling hurricanes, we must rely on relatively rare instances of hurricanes making landfall in areas where sufficient observations are available for surface analysis. In an effort to enhance observations of landfalling storms, the Hurricane Strike Project was initiated in 1978. The landfall portion of Strike incorporates chase teams to record radar data from the closest National Weather Service coastal radar station and to collect poststorm surface meteorological data from available sources. This program was successfully launched in Hurricane Frederic (1979). Data collected by the chase teams and research aircraft data from offshore were analyzed to determine the transition of the surface wind field and precipitation (radar) structure as the storm made landfall (Powell, 1982; Parrish et al., 1982).

In the Hurricane Frederic study (Powell, 1982), data were composited over two time periods to evaluate the transition of the surface wind field as Frederic proceeded from the open Gulf of Mexico to landfall. Results of the Frederic study indicated a sharp discontinuity at the coastline because of increased land friction, a rotation of maximum inflow from the right rear to the landward side, and evidence of adiabatic cooling over land in the core of the storm. The Frederic wind and radar reflectivity fields (Parrish et al., 1982) were compared with Fujita's (1979) damage vector analysis, revealing that some of the most severe damage was probably associated with strong downward bursts of momentum in intense eyewall convection on the landward side of the storm. As a simple aid for forecast guidance during landfall, rough relationships were established between over-water and over-land surface winds and flight-level winds in the same positions with respect to the center of Frederic.

The hurricane landfall program was again put in action as Hurricane Alicia approached the Texas Gulf coast on 18 August 1983. Hurricane Alicia's landfall in the urban Galveston–Houston area made it the third most costly hurricane in U.S. history after Hurricanes Agnes (1972) and Frederic (1979) (Savage et al., 1984). Surface wind data were collected from numerous National Weather Service and private sources. The precipitation structure of the storm was investigated by airborne and land-based radars at Galveston, College Station, and Corpus Christi. Alicia's slow motion before landfall allowed ships of opportunity sufficient warning to clear the area resulting in poor surface data coverage over water compared with that for Frederic. However, data coverage over land was excellent. Surface observations in the Galveston and Houston urban areas were supplemented by an abundance of air quality monitoring stations associated with the petro–chemical industry. These stations made it possible to evaluate the structure of the storm several hours after landfall; such an evaluation was not possible over the rural areas of Mississippi in Frederic.

Collection of the Alicia dataset was seen as an opportunity to extend the detailed study of landfalling hurricanes that was begun with Frederic. The long-term objective of these studies is to establish a framework and database to evaluate the effects of landfall on the momentum, heat, and moisture budgets to characterize a conceptual model of the landfalling tropical cyclone. The objectives of this study are to: 1) document the structure of the surface momentum, precipitation (radar reflectivity), and temperature and humidity fields and their changes during the landfall of Hurricane Alicia; 2) determine physical processes associated with changes in the kinematic and thermodynamic structure at the surface during landfall, including the role of enhanced surface friction at landfall and loss of the surface heat and moisture source; 3) evaluate the asymmetric components of the wind field induced by landfall; 4) determine relationships of the offshore, near-coast aircraft wind to the over-land coastal wind observations for possible use in forecast guidance; and 5) relate the surface wind and radar reflectivity fields to the damage field to identify the most destructive features of landfalling storms.

2. Procedure

a. Storm history

Alicia developed from a low pressure trough in the northern Gulf of Mexico into a tropical storm at 1800 GMT 15 August 1983 in the central Gulf of Mexico about 350 km south of New Orleans. Alicia became a hurricane at 0000 GMT 17 August while moving slowly northwestward at 2–5 m s^{-1}. The track of the center of the low-level storm circulation was determined from aircraft and surface wind data and is shown in Fig. 1. The track indicates that the storm stalled several times, during which radar fixes of the center indicated a looping motion. Further information on the life cycle and development of Alicia can be found in Case and Gerrish (1984).

b. Database

Observation platform locations over water and land are shown adjacent to the storm track in Fig. 1. Over-water data sources consisted of two NOAA research aircraft flights, two oil rig platforms instrumented by the NOAA Data Buoy Center, and several coastal surface observation sites. The aircraft data provided the most complete coverage of the storm and consisted of 30 s averages at the 1500 m level (5000 ft). The aircraft wind data were adjusted to the 10 m level with a diagnostic marine boundary-layer model (Powell, 1980) assuming a neutral stability. NOAA platform data were also adjusted to the 10 m level and consisted of 8.5 min averages. Coastal data consisted of 1 min sustained wind observations from anemometer heights that ranged from 10 to 30 m.

Over-land data sources consisted of hourly data from 85 stations. Many of these stations were National Weather Service and Federal Aviation Administration stations. Valuable supplementary data were provided by private sources, such as Houston Regional Monitoring, Texas Air Control Board, three moored U.S. Coast Guard vessels, Exxon Baytown tower, Dow Chemical at Freeport, and individual observers. In general, wind data were most plentiful, followed by air temperature, surface pressure, and dewpoint temperature. Of the 85 stations, many experienced power outages or evacuations so that only partial records of the storm passage were available. However, only four stations were eliminated by serious equipment errors or exposure problems. The exposure and quality of several of these sources were discussed in detail by Marshall (1984) and Lamberth (1983).

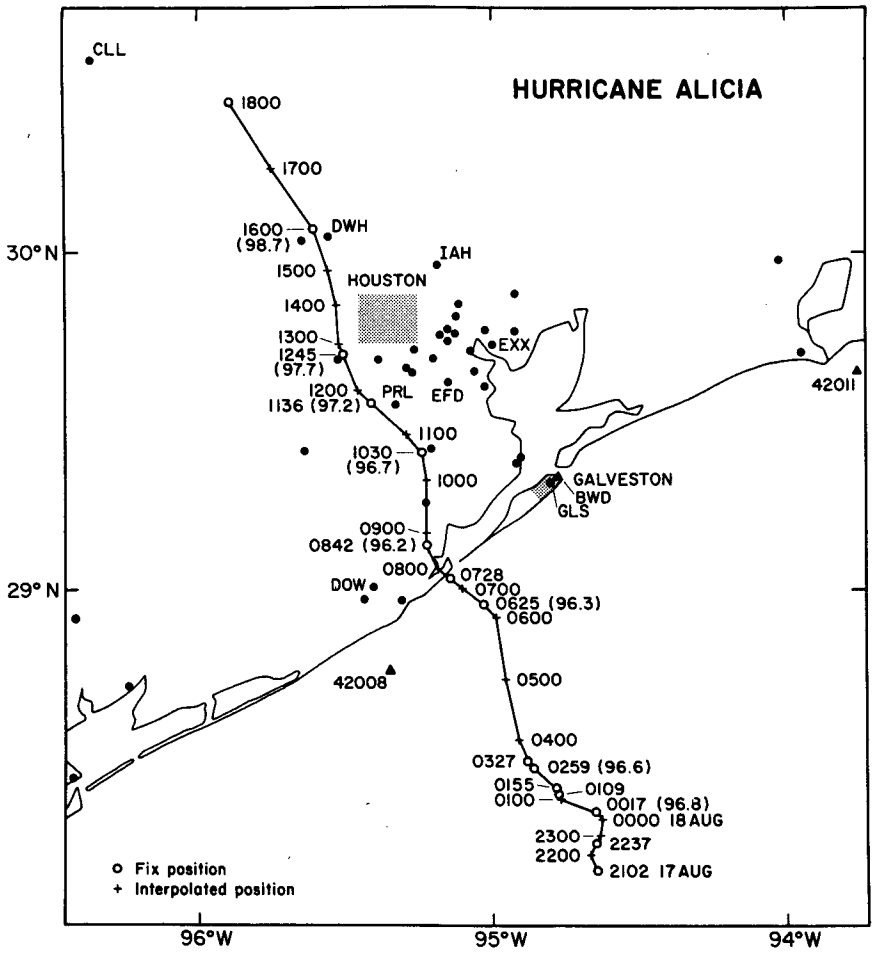

FIG. 1. Hurricane Alicia storm track. Actual wind center fixes are denoted by time in hours and minutes, interpolated positions are given hourly. Minimum sea-level pressures in kPa are denoted in parentheses. Surface wind observation locations are indicated by filled circles adjacent to the track. Buoy and ship locations are denoted by triangles. Station locations referred to in text are (all in Texas) CLL—College Station; EXX—Exxon Baytown; DOW—Dow Chemical; PRL—Pearland; DWH—NW Harris County; EFD—Ellington AFB; GLS—Galveston NWS; BWD—USCG *Buttonwood*.

All anemometer heights were adjusted to 10 m by the logarithmic profile when roughness length estimates were available, or by a power law (Panofsky and Dutton, 1984) based on estimated terrain type when roughness length estimates were unavailable. Anemometer heights ranged from 6 to 14 m, with the exception of the Exxon Baytown site of 37 m. Most National Weather Service and Federal Aviation Administration observations were 1 min sustained winds, unless anemometer charts were available, in which case 10 min averages were determined. The Houston Regional Monitoring sites at 10 m level consisted of 5 min averages. Texas Air Control Board data were at 6 m and consisted of 1 h resultant winds. The Texas Air Control Board data were adjusted to maximum 10 min means using the methods of Durst (1960).

Most temperature and dewpoint data were available from National Weather Service and Federal Aviation Administration sources and consisted of hourly values. Houston Regional Monitoring obtained hourly 5-min averages of temperature (from all sites) and dew point (from 3 sites), from aspirated sensors. Pressure data consisted of hourly values of sea-level pressure from station logs or microbarograph traces when available. Digitized radar data were available from lower fuselage (C-band) radar aboard the NOAA aircraft, a WSR-57 (S-band) radar recorded by a Hurricane Research Division chase team at Galveston (GLS) National Weather Service and an Enterprise (S-band) radar at Texas A&M University at College Station.

Ideally, the spatial sampling of all the fixed platforms should be equivalent to that of the aircraft. According

to Black and Adams (1983), a fixed platform would measure a sampling volume length approximately equal to the sum of the wind velocity and the storm translation velocity, multiplied by the sampling period. A moving platform would measure a sampling volume length given by the product of the aircraft airspeed and the sampling period. For a typical aircraft speed of 110 m s^{-1} it is possible to compute aircraft averaging times that would compare with fixed platform averages in different wind speed ranges. For example, with a wind speed range of 20–40 m s^{-1}, a 1 min fixed platform average would compare with a 10–30 s aircraft average, and a 5 min fixed average would compare with a 55–110 s aircraft average. Aircraft averaging periods must be <60 s, however, to preserve radial resolution in regions of strong velocity gradients; hence, a 30 s aircraft average was chosen as the longest practical sampling period. The fixed platform data used here represent 1, 5, 8.5 or 10 min averages centered on or before every hour. When available, supplementary observations were used between the hourly observations to provide higher resolution in high wind and rainband areas. No systematic differences were detected among the stations because of averaging periods of <10 min; hence, no attempt was made to standardize observations to a particular averaging time. Possible differences caused by exposure were smoothed out in the analysis of the composite data.

c. *Compositing technique*

The study of hurricane landfall is often hampered by lack of sufficient data coverage, especially from rural areas. This problem is compounded by instruments having different exposures, measurement heights, sampling rates, and methods of measurement. In addition, anemometer equipment often fails at the crucial time of the highest winds. These problems were minimized in Alicia by acquiring a relatively dense network of wind observations in the Houston–Galveston areas and compositing the data with respect to the wind center of the storm. An example of the data coverage produced by the composite technique for the landfall period is presented in Fig. 2.

Detailed information on the compositing technique is available in Powell (1982). A critical assumption of this analysis technique is that during the period of the composite, the storm should be near "steady-state" with minimal changes in intensity and structure. The analysis is then assumed to be representative of a mesoscale analysis at the midpoint of the composite period.

The three 8 h periods chosen to depict Alicia's wind structure were: 1) before landfall from 2100 GMT 17 August to 0400 GMT 18 August, during which the minimum sea-level pressure dropped slowly from 96.8 to 96.6 kPa; 2) at landfall from 0400 to 1100 GMT 18 August, during which the central pressure continued to drop to 96.2 kPa at 0840 GMT and then rose to 96.7 kPa at 1030 GMT; and 3) postlandfall with the storm inland from 0900 to 1600 GMT, during which the central pressure filled rapidly to about 98.2 kPa.

According to the changes in minimum sea-level pressure, only the prelandfall and landfall periods were representative of the storm in near-steady-state conditions. Although the pressure rises during the postlandfall period were large, the wind and precipitation structure of the storm showed slower changes and this period was considered to be representative of a weakening hurricane.

3. Results

In this section analyses of the kinematic structure of the flow during the prelandfall, landfall and postlandfall periods are presented, with special emphasis on landfall. The asymmetric structure of the surface wind field is related to components produced by the storm translation, frictional effects, and environmental flow. Finally, the thermodynamic structure of the storm is discussed based on surface analyses of temperature and dewpoint before and after landfall, and flight-level data before and up to landfall.

a. *Kinematic structure*

1) PRELANDFALL

The prelandfall composite (Figs. 3a and 3b) at 0030 GMT consists of Galveston land based radar reflectivity structure and flight-level (1500 m) wind measurements and is representative of the structure of the storm in the open Gulf of Mexico. Figure 3a indicates that Alicia displayed a nearly circular eyewall with a diameter of 28 km. The wind speed maximum was 45–50 m s^{-1} in the north and west sides of the eyewall (Fig. 3b). Airborne Doppler radar wind analyses by Marks and Houze (1985) indicate a level of maximum wind speed near 1500 m and inflow from flight level to 400 m (the lowest level available). Unfortunately, airborne Doppler radar wind measurements were not available for the landfall or postlandfall time periods. Comparisons with National Data Buoy Center platforms indicate that the 10 m wind speeds were 75%–80% of flight-level winds. The 1500 m flight level was well above the top of the hurricane planetary boundary layer (HPBL). The HPBL is here defined to be the upper limit to surface-induced turbulent fluxes of heat, moisture, and momentum, not including fluxes produced by cumulus convection, and is usually 300–500 m deep with the top nearly coinciding with cloud base. Although above the HPBL, the 1500 m level is still within the inflow region of the storm with observations of inflow angles at flight level of 15° or more throughout the storm and 30° or more at the surface. At this time the storm was stalled and slowly strengthening, with a central pressure of 96.7 kPa, but still several hours from landfall. Me-

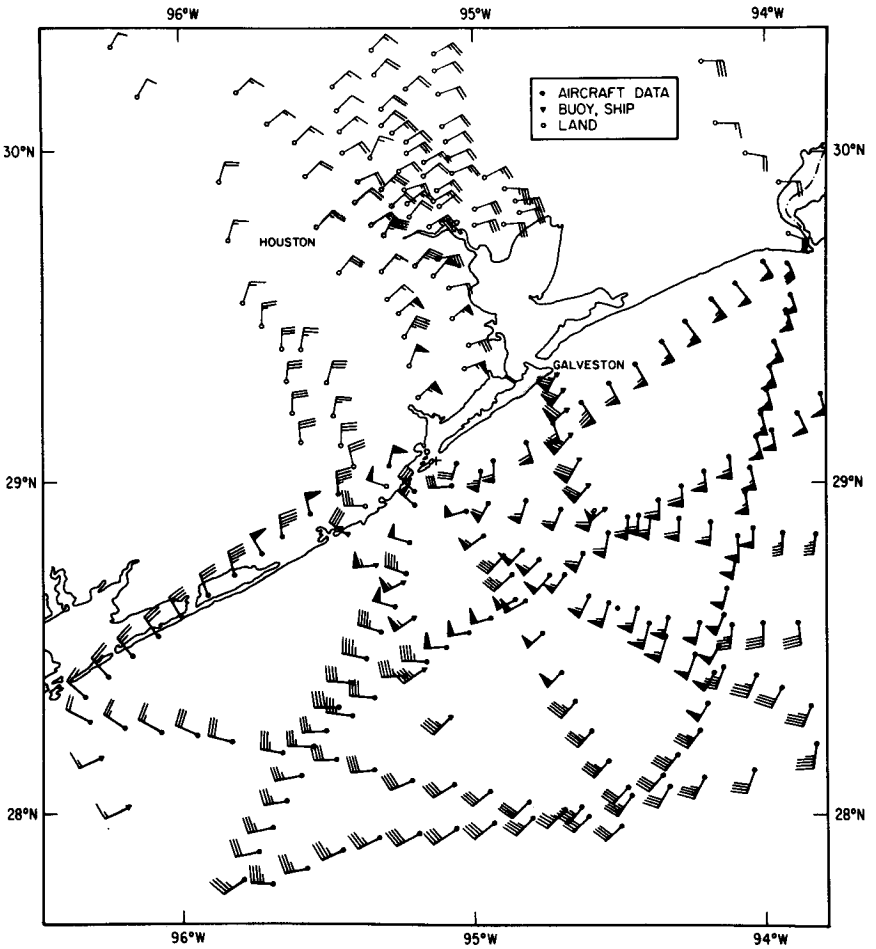

FIG. 2. Example of surface (10 m) wind observations plotted with respect to the storm during the period of the landfall composite, 0400–1100 GMT 18 August 1983. Geography is for 0730 GMT storm position. Some of the data from densely plotted regions were removed to clarify the presentation.

soscale wind maxima were associated with outer rainbands which, because of their circular appearance in Fig. 3a, were believed to represent the outer ring of a concentric double eyewall as reported by Willoughby (1985).

2) LANDFALL

The composite surface wind and radar reflectivity structure of the storm at landfall (0730 GMT) is depicted in Fig. 4. Figure 4a shows that the eyewall was open (minimum reflectivity) to the south and maintained a 28 km diameter. Outer rainbands were still nearly concentric to the eyewall and stratiform (horizontally uniform in reflectivity), with some cellular activity west of Galveston Bay and offshore to the east of the center. The outer rainband offshore Galveston Island in Fig. 4a moved outward at about 7 m s^{-1}, but was replaced by a subsequent outer band that formed in the same location and moved slowly outward at 2 m s^{-1}. The band reflectivity structures consisted of poorly defined stratiform precipitation with embedded band-shaped reflectivity cells. The surface wind field developed asymmetries from the land–sea frictional differences, which are evident as discontinuities at the coastline.

Flight-level data for this period indicated that the large area of >30 m s^{-1} winds (which actually exceeded flight-level measurements in the eyewall) to the northeast of the storm center was associated with an outer rainband and, indeed, this was the region where the maximum sustained surface winds of 39 m s^{-1} were measured by the USCG vessel *Buttonwood*. In fact, in the four instances when the aircraft flew offshore, parallel to Galveston Island, peak gusts at BWD exceeded peak 2 s gusts measured by the aircraft at 1500 m level. Unfortunately, aircraft measurements were unavailable from the right front quadrant of the eyewall where

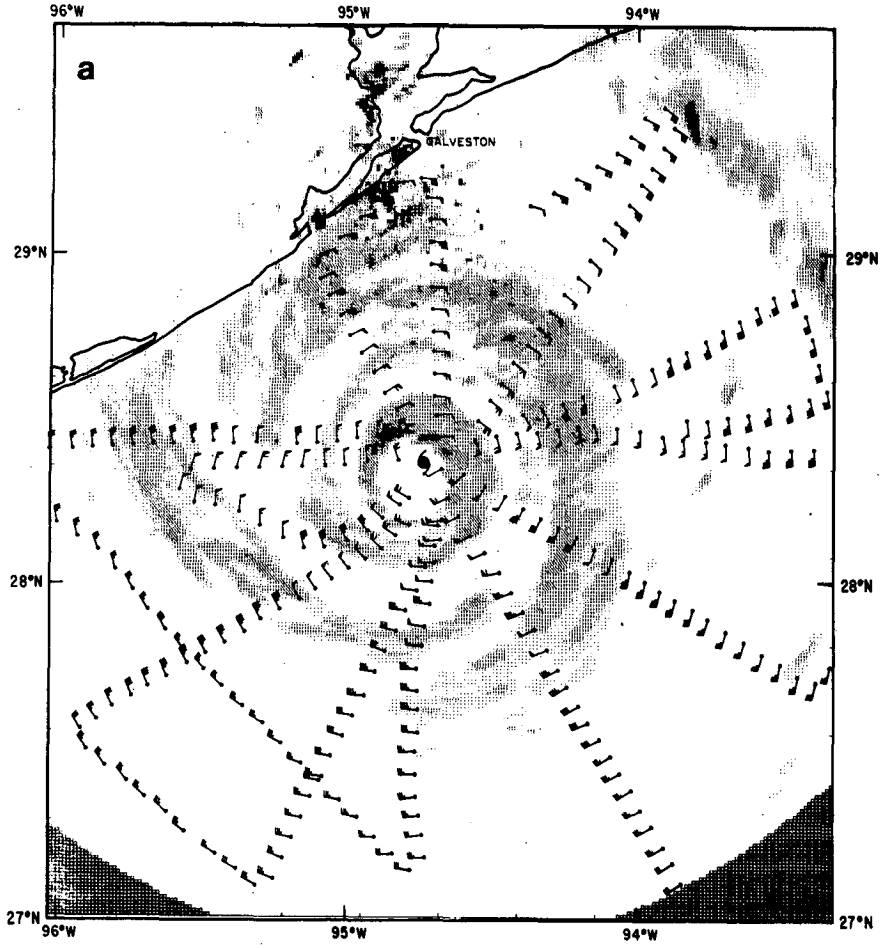

FIG. 3a. Example of flight level (1500 m) observations that went into the prelandfall streamline and isotach analysis of Fig. 3b, and radar reflectivity map from Galveston National Weather Service Office at 0036 GMT 18 August 1983. Reflectivity contours are at 24, 28, 33, 38 and 43 dBZ corresponding roughly to rainfall rates of 0.9, 1.7, 4.0, 9.6, and 22.4 mm h^{-1}.

maximum winds had been measured (Fig. 3b) at about 0100 GMT. However, a careful look at additional surface data (shown in the isotach and streamline analyses in Fig. 4b), with damage analyses after Stiegler (1983) in Fig. 4c, indicate that the maximum surface winds, as well as the most destruction, were still associated with the eyewall in the right front quadrant of the storm.

In agreement with studies of tornadoes in hurricanes by Novlan and Gray (1974) and Gentry (1983), most of the tornadoes in the storm occurred during the landfall period in the quadrant of the onshore flow (northeast quadrant). Tornado positions [numbered in order of occurrence as published in *Storm Data* (1983)], are shown in Fig. 4a and indicate that most of the tornadoes were produced in the outer rainbands as they impinged on the area west of Galveston Bay. Indeed, of the 15 tornadoes that occurred during the three composite analysis periods, 13 could be attributed to outer rainbands.

The surface wind field in Fig. 4b was digitized to a cylindrical coordinate system over a 160 × 160 km domain with grid points every 16 km in radius and every 10° in azimuth to compute fields of radial and tangential wind, divergence, and inflow angle at 0730 GMT. The mesoscale flow features associated with the outer rainband offshore Galveston Island and the land–sea frictional asymmetry are again evident in further analyses in Figs. 5a through 5c. The surface divergence field in Fig. 5c distinguishes this region with a couplet of divergence and convergence on the inner and outer sides of the eastern outer rainband, respectively. The small divergent region is associated with a minimum in radar activity and air bypassing the eyewall to feed the rainband. The differences between surface and flight-level flow are illustrated by trajectories (Fig. 4a) of air parcels at each level from the coast on the southwest side to the outer rainband on the east side of the storm at 0730 GMT. The flight-level trajectory is nearly circular due to low inflow angles and small variation

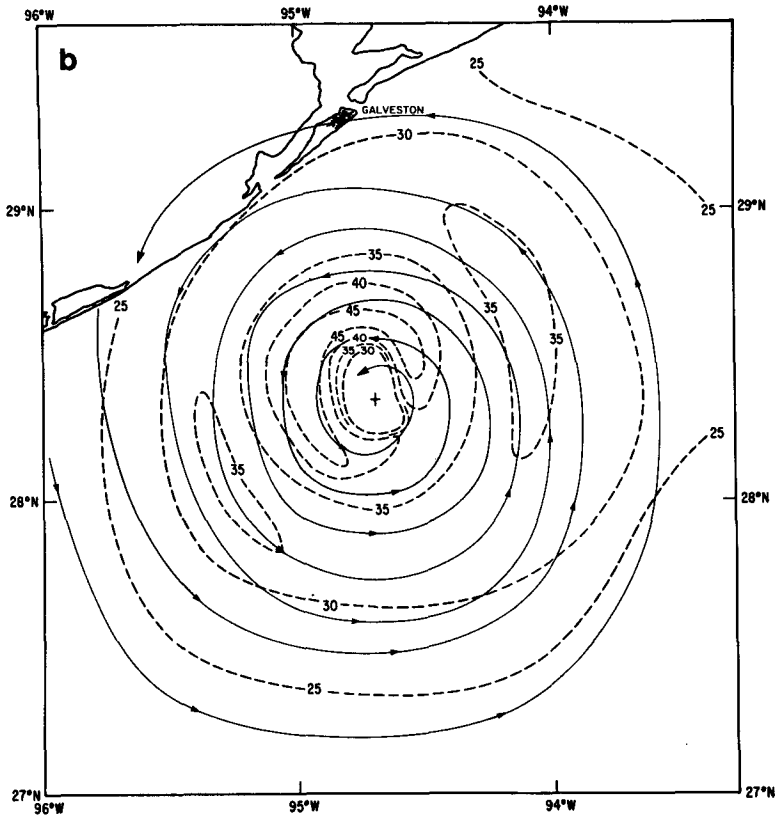

FIG. 3b. Prelandfall flight-level streamline and isotach composite analysis centered on 0030 GMT 18 August 1983. Speeds are in meters per second.

in wind speeds, while the surface air undergoes an acceleration immediately off the coast, proceeding as strong inflow into the storm changing to inflow into the outer band around 0700 GMT.

At flight level (not shown), the area just offshore GLS showed a weaker couplet of divergence and convergence on the inner and outer edges of the rainband, respectively. However, the radial wind component (Fig. 6a) remained negative as the flow continued inward. The weak flight-level convergence contrasted with the Hurricane Floyd rainband studied by Barnes et al. (1983), which displayed maximum convergence at the 1500 m level.

Another notable aspect of the wind field was the increase in radial component and decrease in tangential component as the flow proceeded from land to sea on the southwest side of the storm. The over-land flow tended to come off the land perpendicular to the coastline, but the flow over the water tended to parallel the coastline. Hence, the divergence field in Fig. 5c shows confluence and convergence on both sides of the storm in contrast to wind analyses made in Hurricane Frederic (Powell, 1982) and also model simulations (Tuleya and Kurihara, 1978; Tuleya et al., 1984; Moss and Jones, 1978). These studies indicated convergence to the right of the storm center, but divergence and minimum inflow in accelerating offshore flow to the left of the storm at landfall. A portion of the region of surface convergence on the southwest side of the storm was coincident with outer rainbands (Fig. 4a), which formed in the area just offshore.

The fact that some of the mesoscale features that are present so strongly at the surface are only weakly present, or not present, at flight level, has implications both for the dynamics of the rainband and the utility of reconnaissance observations for diagnosing surface conditions. Radial profiles of flight level radial and tangential wind, D-value (the difference between the radar altitude and the pressure altitude), and the difference between flight level and surface radial and tangential wind components at 1500 m are presented in Fig. 6. These profiles are northeast and southwest of the center extending just offshore parallel to the coast. Both profiles show the double wind maxima in the tangential winds and a flattening of the D-value profile (box, in Fig. 6) near the inside edges of the rainbands. In agreement with Barnes et al. (1983), the flattening is associated with minima in the radial and tangential wind on the inside of the band. The slope of the radial wind profile shows divergence on the inside edge of the band. The radial wind profile on the northeast side of the storm shows inflow at flight level above surface

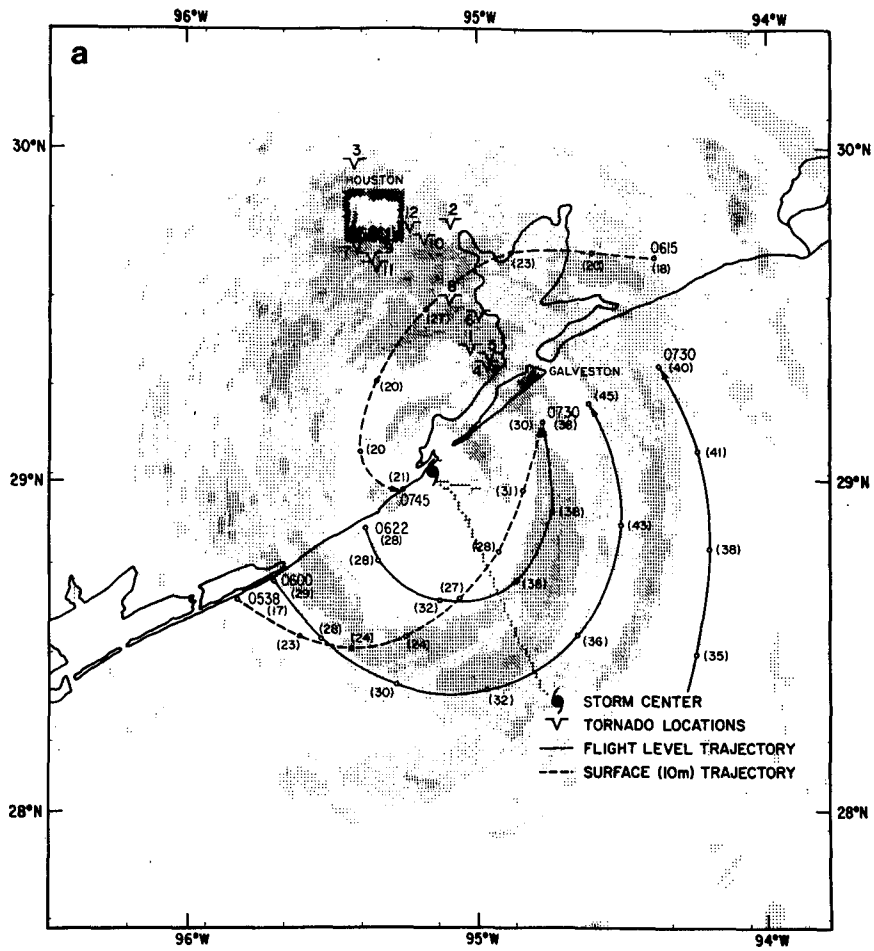

FIG. 4. (a) As in Fig. 3a but from a composite of the airborne lower fuselage radar from 0716–0731 GMT. Trajectories of surface (10 m) air (dashed line) and flight level (solid line) with start and end times and wind speeds (in parenthesis). Times (GMT) of tornadoes (v) are: 1) 0310; 2) 0330; 3) 0359; 4) 0440; 5) 0440; 6) 0443; 7) 0702; 8) 0715; 9) 0745; 10) 0802; 11) 0820; 12) 0830. (b) Landfall composite analysis for the 10 m level centered at 0730 GMT. (c) Damage vector directions, Fujita damage scales (after Steigler, 1983) and surface (10 m) streamlines from the landfall composite.

outflow ($\Delta V_r < 0$) and on the southwest side the flight-level data show outflow above surface inflow ($\Delta V_r > 0$). On the southwest side, the overwater flow parallel to the coastline displayed strong radial inflow. Such inflow may have been produced in part by a south-southwest environmental flow roughly parallel to the southwest–northeast coastline orientation. (This characteristic is discussed in section 2b.)

On the northeast side, the environmental flow would act to reinforce outflow, but it is still difficult to explain why the surface flow was outward while the flow at 1500 m was inward. An inspection of surface wind observations from Galveston National Weather Service (GLS) and the U.S. Coast Guard vessel *Buttonwood* (BWD) (5 km northeast of GLS), showed a wind shift from the southeast (surface inflow) to the southwest and west (surface outflow) that lasted from 0830 to 1300 GMT. Some of the BWD observations showing southwest winds are plotted in Fig. 2.

Possible mechanisms for surface outflow in this region would include a mesoscale downdraft associated with the outer rainband region and a vortex-scale convergence line produced at the axis of the outer concentric rainband. Analyses of the three-dimensional reflectivity structure (not shown) were constructed from airborne tail radar data that were collected during flight legs parallel to Galveston Island at 0730, 0950, 1030 and 1150 GMT. These analyses show evidence of a downdraft spreading below flight level from the leading edge of the outer band toward GLS and BWD at 0730. Such a downdraft could affect the surface flow without influencing flight-level winds. This band moved outward at 7 m s^{-1}, and subsequent bands continued to form in this region with slow outward movement, but

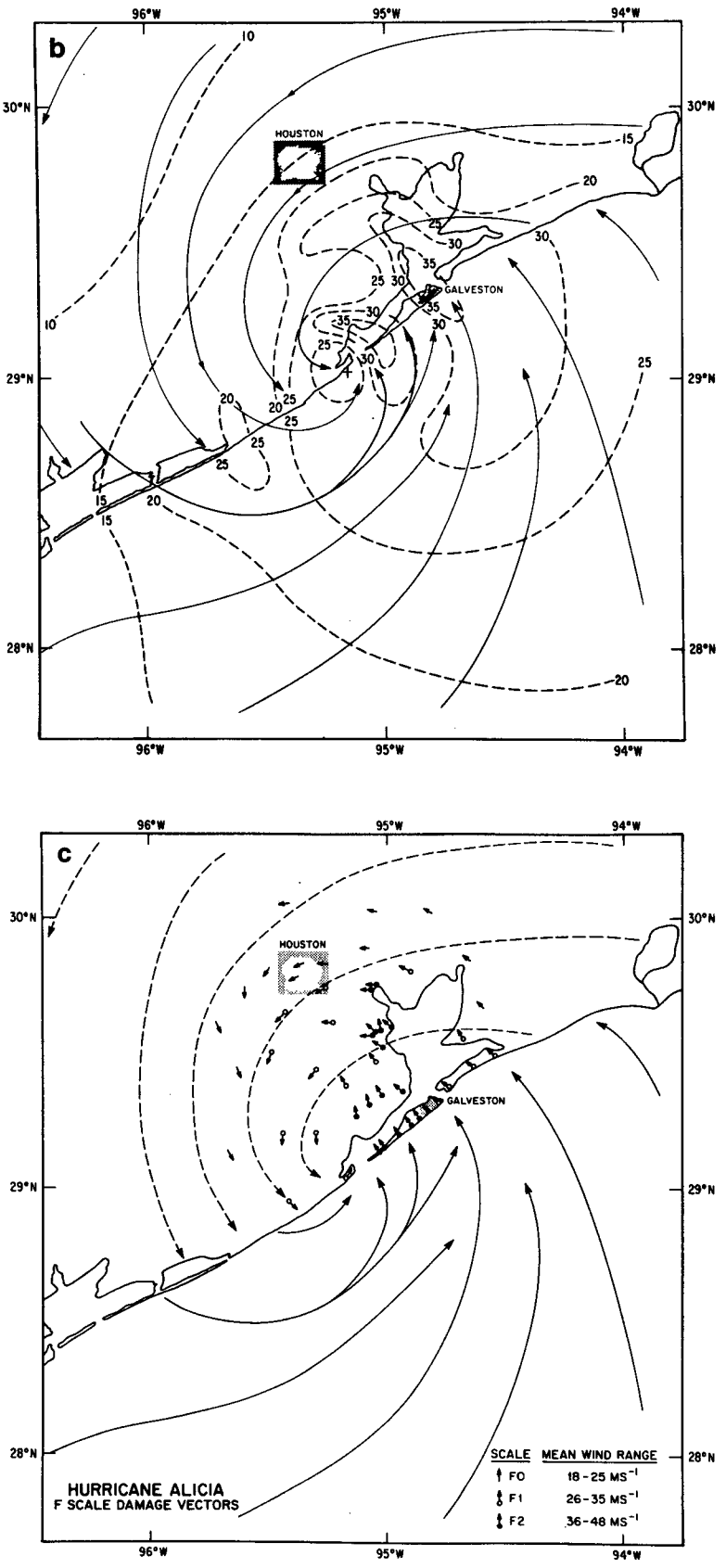

FIG. 4. (*Continued*)

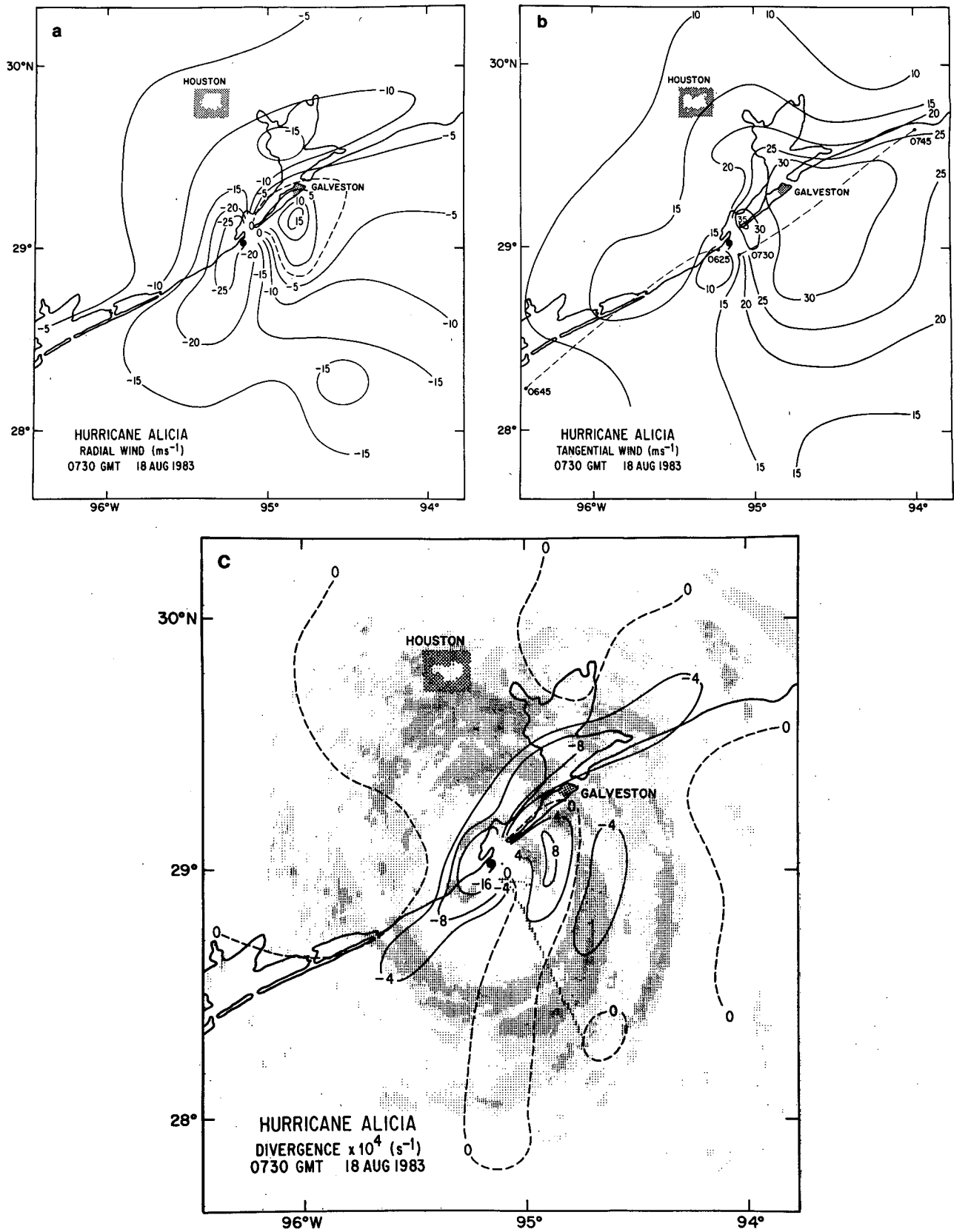

FIG. 5. (a) Radial and (b) tangential, surface (10 m) wind fields for the landfall composite. Negative radial component indicates inflow. Dashed lines in 5(b) refer to portions of flight level data used in Fig. 6. (c) Surface divergence field for the landfall composite. Stipling indicates radar reflectivity field in Fig. 4a.

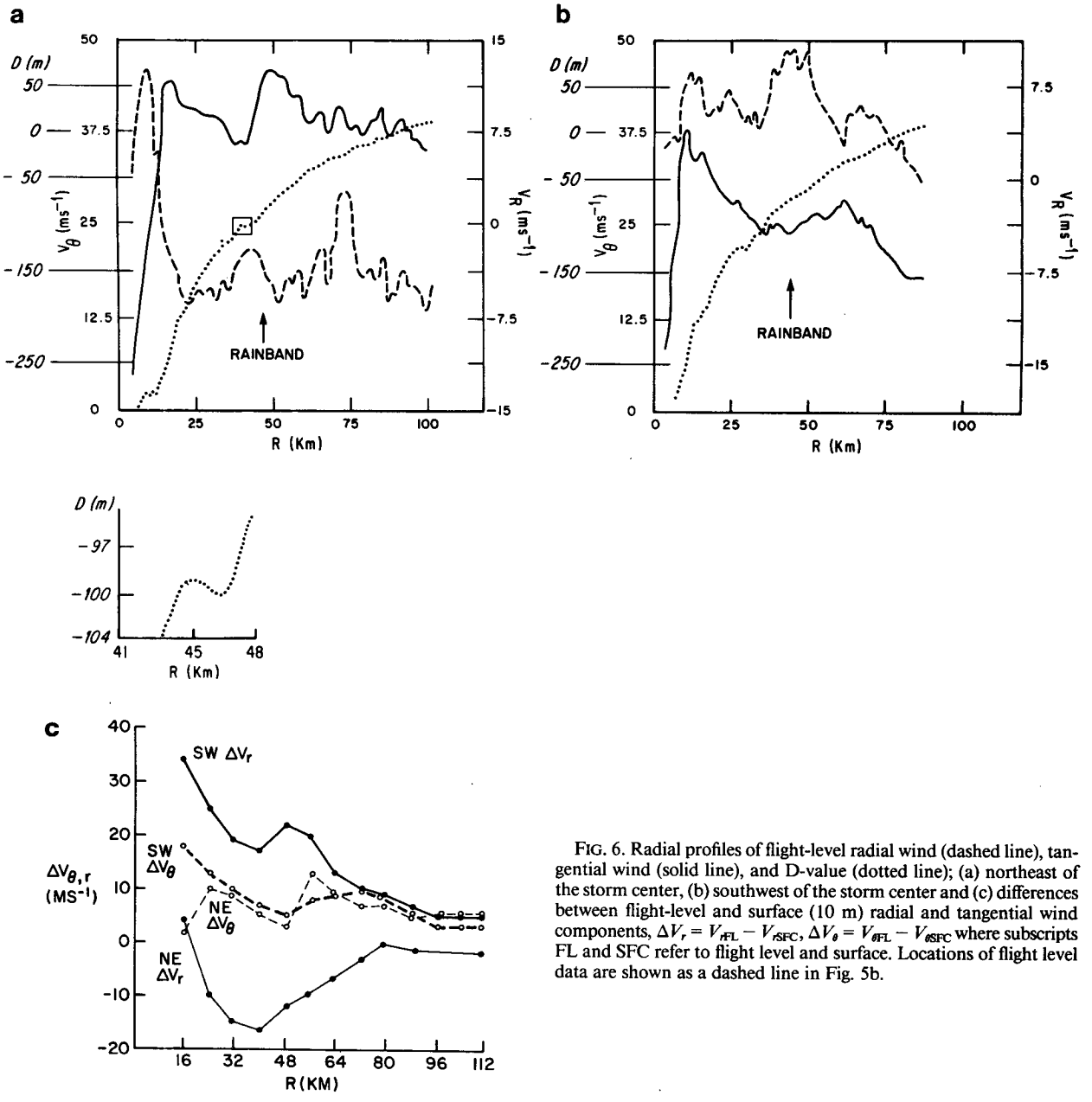

FIG. 6. Radial profiles of flight-level radial wind (dashed line), tangential wind (solid line), and D-value (dotted line); (a) northeast of the storm center, (b) southwest of the storm center and (c) differences between flight-level and surface (10 m) radial and tangential wind components, $\Delta V_r = V_{rFL} - V_{rSFC}$, $\Delta V_\theta = V_{\theta FL} - V_{\theta SFC}$ where subscripts FL and SFC refer to flight level and surface. Locations of flight level data are shown as a dashed line in Fig. 5b.

there was no evidence of spreading downdrafts. A downdraft within the outward moving rainband may have been responsible for initiating the windshift, but could not have persisted for the several hours during which surface outflow occurred.

The surface outflow was initiated when an outer band passed the northeast end of Galveston Island at 0730 GMT and persisted until the southeast edge of the outer band region (moving with the storm) passed the island after 1300 GMT. The time scale of the surface outflow indicates that a vortex-scale mechanism may have produced the outflow. Flight-level radial profiles of tangential wind, radial wind, and equivalent potential temperature at 0730 and 0950 GMT indicate a secondary wind maximum in the outer band region associated with convergence as determined from the radial wind profile. On the inside of this maximum in the core region, equivalent potential temperature (θ_e) was about 350–353 K, while on the outside, θ_e decreased sharply to 344–345 K. At landfall, it appears that the axis of the outer rainband region was associated with strong surface convergence that was producing an obstruction to the surface flow and preventing air outside the band from flowing through the band and con-

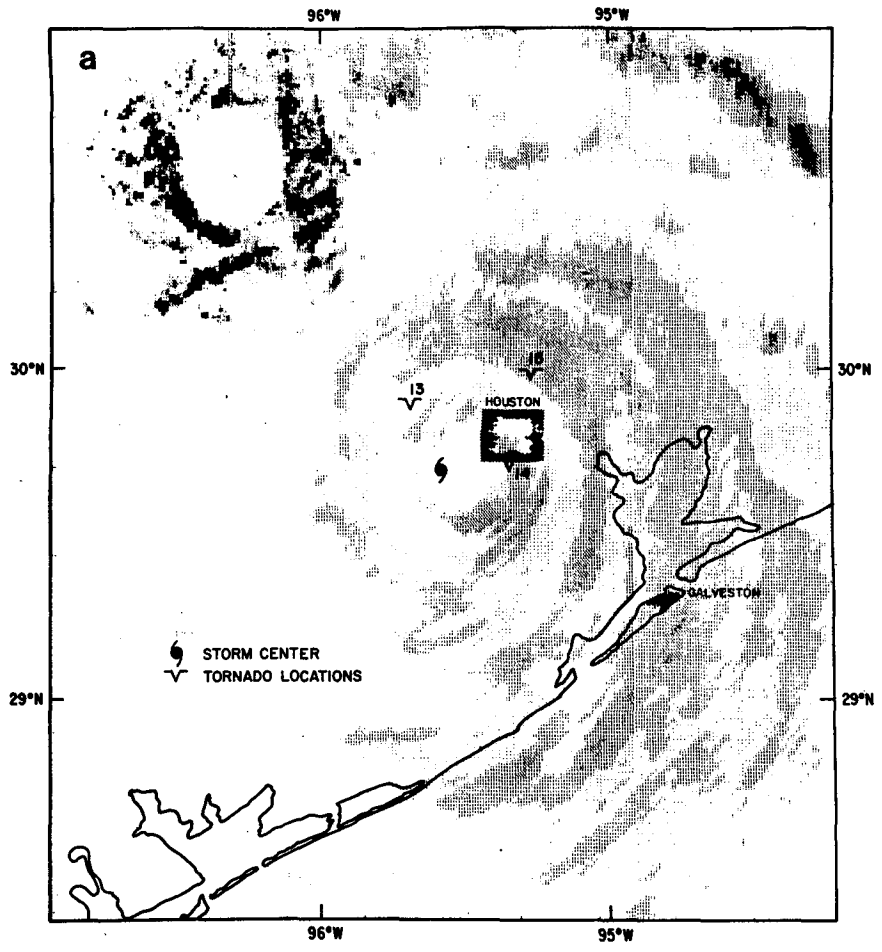

FIG. 7a. Radar reflectivity as in Fig. 3a, but from the Texas A&M radar at 1244 GMT. Times (GMT) of tornadoes are: 13) 1020; 14) 1105; 15) 1220.

tinuing into the eyewall. This feature was not evident in prelandfall Doppler wind analyses at the 400 m level in the same relative location. Its initiation at landfall may be indicative of a vortex-scale readjustment of the wind field in response to increased surface roughness. A partial obstruction was seen by Barnes et al. (1983) in a principal rainband in Hurricane Floyd, but the effect was greatest at the 1500 m level where the maximum inflow and convergence were located.

According to Willoughby et al. (1984), the rainband acts as a boundary, delineating the transition between the core region and the environment surrounding the storm. His results indicate that, at 85.0 kPa (1500 m), the air inside the principal rainband tends to remain with the storm's core, while the air outside the rainband represents the environment through which the storm moves. In the case of Alicia, at 85.0 kPa, the outer rainband acted as a thermodynamic boundary between higher θ_e air of the core and lower θ_e air in the environment. The higher θ_e core appears to originate from boundary-layer mixing in the core convection. Surface flow trajectories in Fig. 4a show that the core is supplied by strong over-water inflow from the southwest and overland inflow on the northwest and north sites. On the east side the previously mentioned obstruction feature acts as a kinematic boundary between the well-mixed boundary layer air of the core and the outside, lower θ_e, "environmental" air. At 85.0 kPa flow trajectories over water (Fig. 4a) are nearly circular indicating little lateral mixing and a maintenance of the transition region between the core and the environment.

It is important that forecasters be aware that large differences can occur between flight level and the surface, especially when flight level is above the top of the boundary layer. Although the level of maximum horizontal wind speed is usually between 1000 and 1500 m, there is some airborne Doppler radar evidence (Powell and Black, 1984) that the level of maximum wind in the vicinity of rainbands can occur at low levels (300–500 m). In such a case, the surface would be much closer to the strongest wind level and larger differences

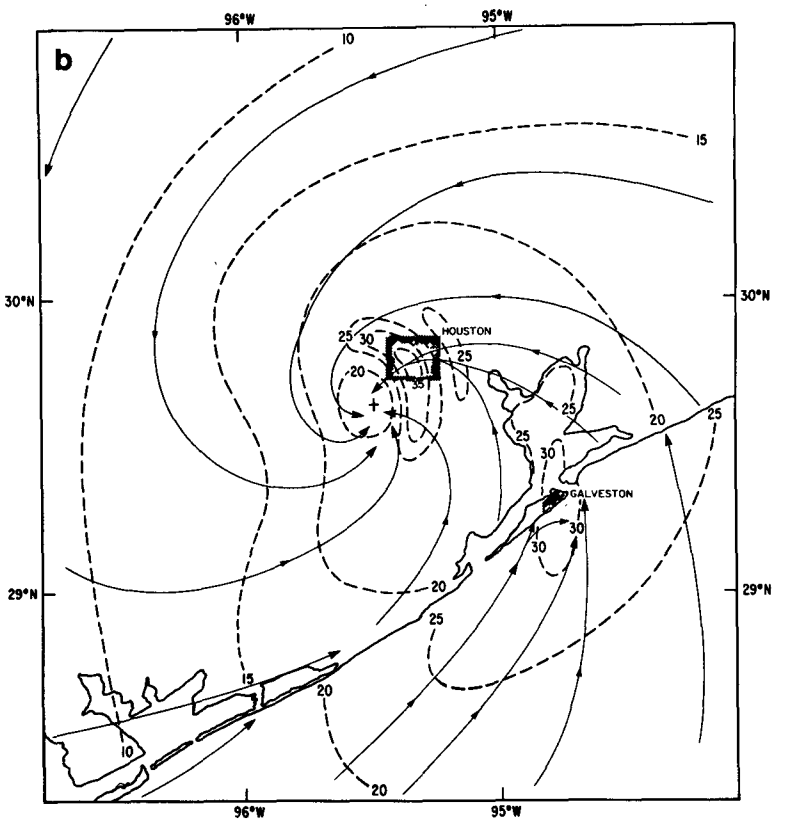

FIG. 7b. As in Fig. 4b, but for the postlandfall composite centered at 1230 GMT.

could occur. Perhaps this is why the surface gusts measured at the *Buttonwood* exceeded flight-level peak gusts during each of the four offshore aircraft passes.

3) POSTLANDFALL

Due to the proximity of Houston as the storm progressed inland, sufficient data were available for postlandfall wind and radar reflectivity analyses, shown in Figs. 7a and 7b, centered at 1230 GMT. At this time the storm continued to move northward at 5 m s^{-1} and the central pressure had filled to 97.7 kP. Figure 7a shows that the eye diameter remained at 28 km, but was open to the southwest. The highest radar reflectivity was in the southeast and northwest portion of the eyewall. On the east side, the outer rainband region remained stratiform, with embedded band-shaped higher reflectivity cores. The axis of this region extended from north-northeast to south-southwest through Galveston Bay, Galveston Island, and offshore. The tornado positions shown in Fig. 7a were associated with passage of the eyewall. The eye started to fill rapidly after 1030 GMT (from 96.7 kP at 1030 GMT to 98.2 kP at 1600 GMT). Some weakening of the wind field is indicated by the decreased area enclosed by the higher wind speed isotachs in Fig. 7b, when compared with Fig. 4b. Unfortunately, no direct wind measurements were available from downtown Houston during this period; therefore, the analysis in Fig. 7b is based on earlier measurements at 1100 GMT. Wind observations from Pearland (10 mi south of Houston), indicated that maximum winds in the eyewall were close to 35 m s^{-1} at 1100 GMT and measurements from Ellington Air Force Base (10 mi southeast of Houston) were 30 m s^{-1} on the outside edge of the eyewall at 1100 GMT. Shortly afterward, from 1130 to 1300 GMT, downtown Houston experienced extensive window damage during the passage of the eyewall. Although the central pressure was rising rapidly, sustained hurricane-force winds were maintained in the eyewall 5 h after landfall. Perhaps the eyewall pressure gradient did not respond immediately to the increase in central pressure or active eyewall convection provided additional momentum to support strong winds. Later eyewall observations from northwest Harris County (Texas Air Control Board) at 1430 GMT (21 mi north of Houston) indicate that the storm had weakened considerably after passing Houston, having only 20 m s^{-1} winds in the left front quadrant of the eyewall and 25 m s^{-1} winds in the right front quadrant. These winds were measured at Houston Intercontinental Airport (16 mi north) at 1400 GMT.

The outer wind maximum of 25 m s^{-1} to the northeast of the storm center was associated with the outer

rainband region. Surface outflow in the vicinity of Galveston persisted until 1300 GMT, after which the outer band axis moved northwest of Galveston Island and surface inflow prevailed on the outside of the band axis.

b. *Asymmetric surface flow structure*

As seen from the surface streamline and isotach analyses discussed in section 3a, the surface wind distribution of a landfalling hurricane displays an asymmetric structure with features in the divergence field related to the surface roughness and its orientation, the motion of the storm through its environment, the environmental flow field, and the position of convective bands. If the various components of the asymmetric structure of the surface flow could be isolated, it might be possible to determine the effect of each component on the storm structure and dynamics. It might also be possible to predict the evolution of the surface flow field, given the storm intensity and asymmetric components.

Early studies of asymmetrical wind structure by Sherman (1956) and Krishnamurti (1962) indicated that the wind field in a hurricane could not be fully explained by superimposing translation on a symmetric vortex. The effect of vortex motion on the wind distribution at the surface has been investigated by Myers and Malkin (1961), Chow (1971), and Shapiro (1983). Shapiro examined the effect of varying translation speeds on the wind field of a gradient-balance vortex with a slab boundary layer. He hypothesized that a storm translational motion, when added to an axisymmetric vortex, should induce asymmetries in the circulation in the boundary layer, leading to further asymmetries in surface friction, convergence, and convection. In Shapiro's study, the model storm moved with a translational velocity equal to the geostrophic wind caused by a background or environmental pressure gradient. Shapiro's results, and recent work by Ooyama (personal communication, 1985) show excellent agreement between bands of convergence in the model boundary layer and the distribution of radar reflectivity in Hurricane Frederic (1979), Allen (1980), and Debby (1982) over the open ocean. Although Shapiro found good agreement with limited observations from storms in the open ocean, the problem can be complicated by differences between the environmental flow and the storm motion and by frictional differences at landfall.

In an effort to deduce some of the components of the asymmetric surface wind field, the axisymmetric mean surface circulation has been subtracted from the wind field of Fig. 4b to form the perturbation wind field shown in Fig. 8a. This field consists of asymmetries that were produced by the land–sea frictional difference, storm motion, environmental flow, and convective effects. A similar analysis of the relative wind perturbation field (not shown) produced a nearly identical streamline field with weaker speeds on the right and stronger speeds on the left, as expected. The land–sea asymmetry should induce an anticyclonic flow over land and cyclonic flow over water. This flow counteracts the mean vortex over land where winds are weaker than the mean, because of friction, and reinforces the mean circulation over water where the winds are greater than the mean. The anticyclonic flow over land can be seen in Fig. 8a, but cyclonic flow over the water is only present just offshore, northeast of the center.

The storm motion was toward 335° at 5 m s^{-1}. The storm motion should act to increase surface winds to the right of the direction of motion and decrease winds to the left. The background geostrophic flow (computed from sea level pressures on a 10° latitude–longitude grid centered on the storm in Fig. 9) was from 205° at 4 m s^{-1}. The environmental flow from southwest to northeast should induce inflow and a component of the flow paralleling the coastline (coastline orientation in this region is 230°) on the southwest side and outflow on the northeast side as shown in the inflow angle field of the total surface flow in Fig. 8b. The environmental flow can be visualized in Fig. 9 as the geostrophic flow that would occur in the absence of the storm. The effect of an easterly surface environmental flow field in Hurricane Frederic (Powell, 1982) was to produce maximum inflow to the east of the storm and minimum inflow on the west side of the storm. This effect can also be seen in the model of the Stationary Band Complex at 85.0 kPa by Willoughby et al. (1984). Unfortunately, the storm motion and environmental flow may be so closely related that separation of these components is difficult.

The largest perturbation velocities occurred on the inside of the outer band to the northeast of the storm center where storm motion and environmental flow reinforce the circulation. Perhaps the combination of these perturbation components led to a surface convergence distribution that resulted in the observed rainband distribution. Asymmetries induced by rainband convection may also affect the flow there, but are difficult to isolate.

c. *Thermodynamic structure and storm decay*

A cooling of the upper and middle levels of the storm is ultimately responsible for the hydrostatic increase in the central pressure necessary to reduce the pressure gradient and weaken the hurricane after landfall. Observational studies and numerical model simulations such as Tuleya and Kurihara (1978) suggest a general sequence of physical and dynamic events leading to decay of a hurricane. At landfall, friction produces an increase in boundary layer inflow and convergence leading to enhanced upward motion. Increased moisture convergence temporarily increases precipitation, but the lack of moisture and heat over land eventually

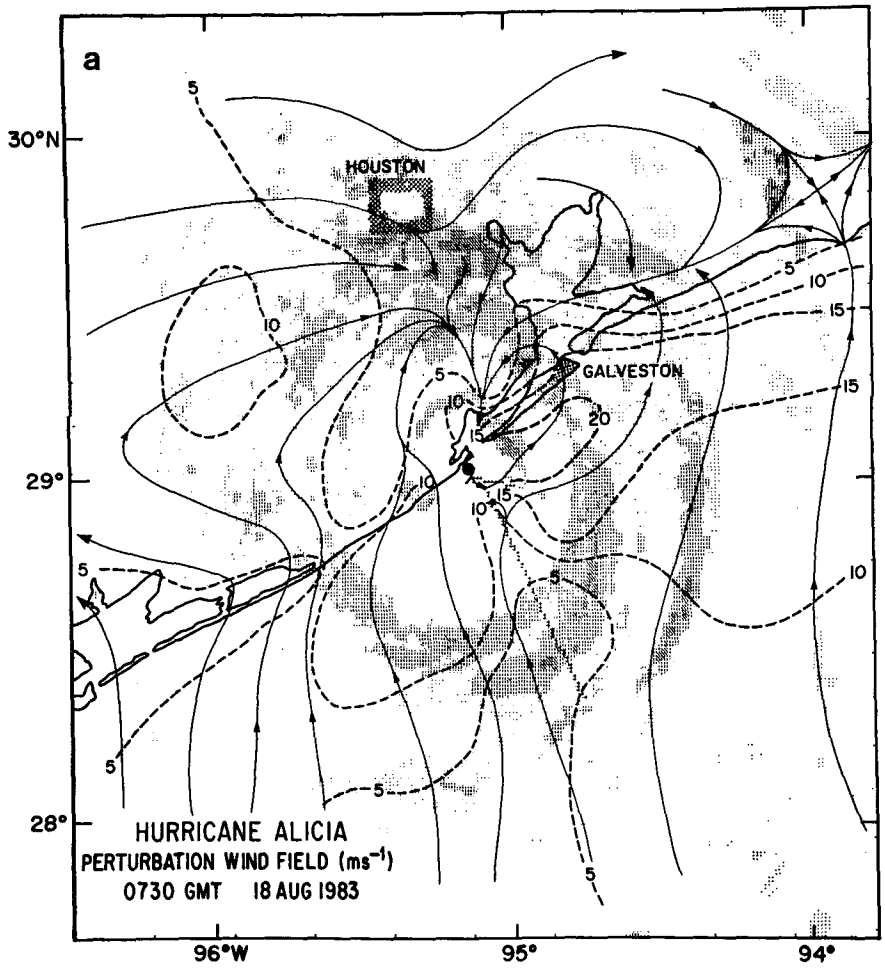

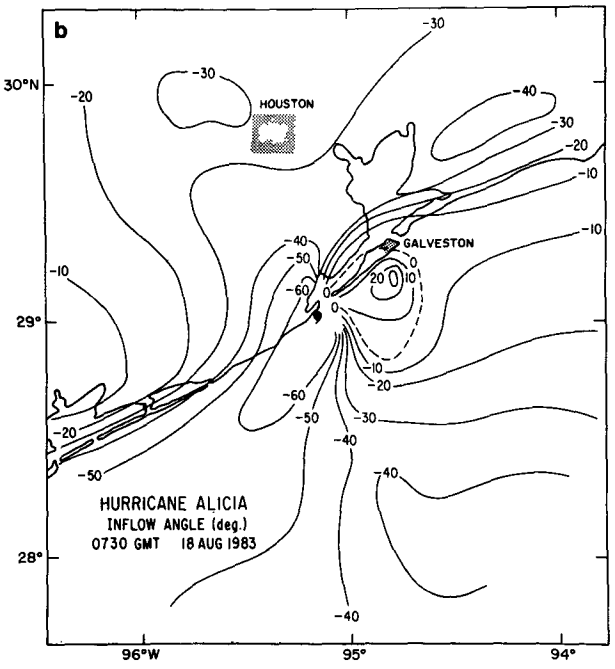

FIG. 8. (a) Perturbation wind field for the landfall composite in Fig. 4b. Stipling is reflectivity field of Fig. 4a. (b) Surface (10 m) inflow angles (in degrees) for the landfall composite. Negative numbers are degrees of inflow with respect to the storm center, positive numbers are outflow.

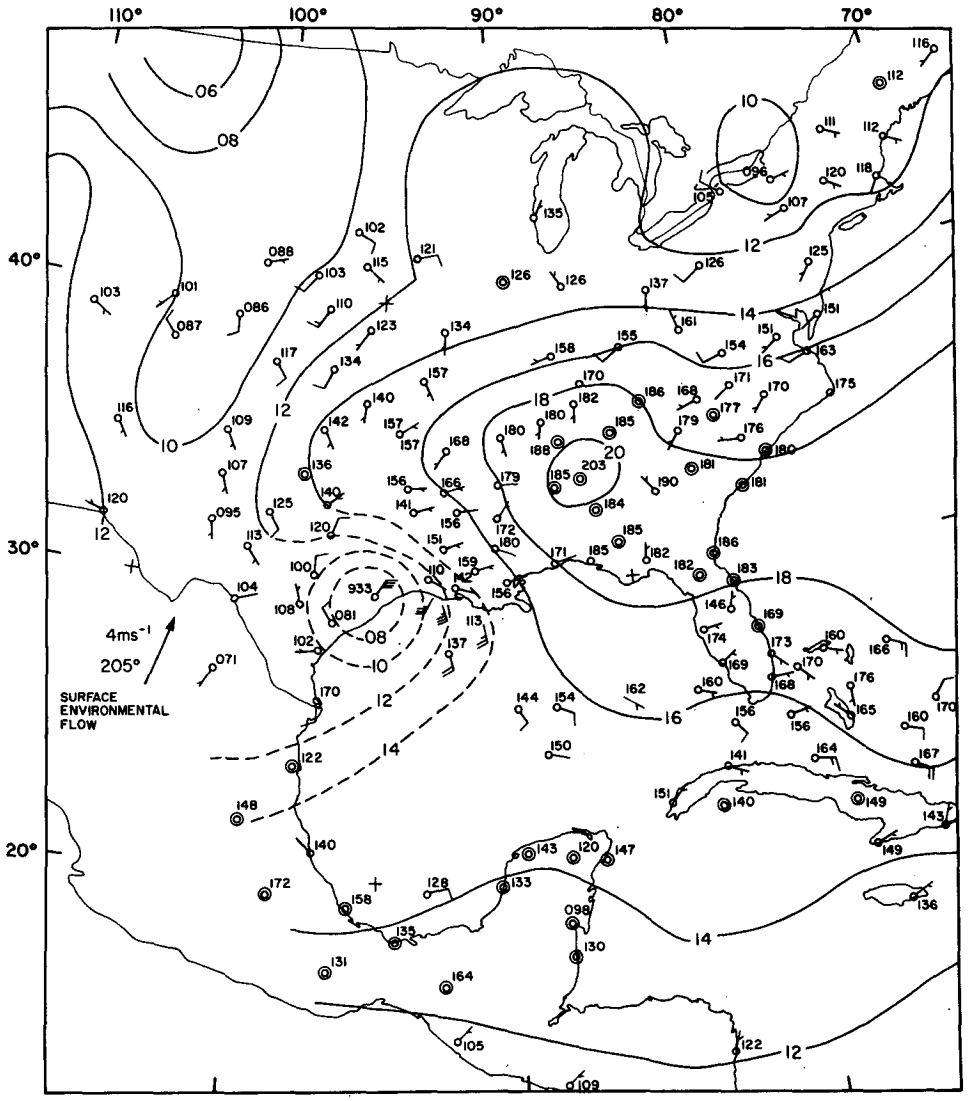

FIG. 9. WMO Regional Center for Tropical Meteorology surface analysis for 1200 GMT 18 August, 1983. Arrow denotes geostrophic wind determined at storm center, from grid point data (locations denoted by +).

reduces middle and upper level diabatic heating in the convection (occurring at lowered θ_e) such that it is exceeded by adiabatic cooling in the upward motion. Hence the middle and upper layers cool due to a decrease in the convective heat source and a corresponding decrease in compensating subsidence. Unfortunately, there were no aircraft observations at these levels and no soundings over land close enough to the core of the storm to document cooling in the middle and upper layers during landfall. Such cooling is initiated in the boundary layer once the hurricane circulation becomes affected by land and may be caused by several possible physical mechanisms. These mechanisms include: 1) loss of the oceanic heat and moisture source, causing air to cool dry adiabatically while flowing toward the center; 2) advection of cooler and drier air from over land; 3) enhancement of rainband convection over land leading to mesoscale saturated downdrafts of cool, relatively dry middle level air; and 4) enhanced turbulent entrainment of dry air from above the top of the boundary layer. The addition of cooler and drier air into the boundary layer leads to inflowing air with relatively low θ_e becoming available for moist adiabatic ascent in the core (inner 100 km) of the storm. Malkus and Riehl (1960) reasoned that a 1.0° increase of surface θ_e could lead to a 0.25 kPa decrease in central sea-level pressure. This decrease in surface pressure could only occur if nearly undilute vertical moist adiabatic ascent of this surface air extended to upper and middle levels in the core of the hurricane. As described in Anthes (1982), such ascent in the core region is only partially responsible for the upper level heating required

for low central surface pressures. The primary mechanism for the upper level heating is compensating subsidence (Shapiro and Willoughby, 1982) produced in response to the convective heat source.

The most important physical mechanism for the weakening of a hurricane at landfall is usually considered to be the absence of surface fluxes of sensible and latent heat. These fluxes depend upon the vertical temperature and moisture gradients between the surface and the air adjacent to the surface. Therefore, a decrease in surface heat and moisture fluxes occurs at landfall because of much lower surface (soil, vegetation, structures, and standing water) temperatures and saturation vapor pressures over land as compared with the sea surface. Miller (1964) observed a 20° decrease in θ_e over 24 h during the landfall of Hurricane Donna (1960). During that time period, the central pressure increased from 94.0 to 97.0 kPa. He determined that the sensible heat and moisture fluxes over land were essentially zero. Hence, the air flowing toward the center of the storm would cool adiabatically and arrive at the core cooler and drier than it would have over open water.

In this section, surface and flight-level composite analyses of the temperature and moisture structure are evaluated to ascertain the processes leading to the filling of Hurricane Alicia. The temperature, especially dewpoint temperature, data coverage, was less plentiful than the wind data and displayed much scatter. Most of the scatter in the temperature field could be attributed to sensor wetting effects causing the temperature measurement to resemble a wet bulb thermometer measurement during heavy rain squalls. Lower dewpoints in the vicinity of rainbands indicated that downdrafts were penetrating the boundary layer. Using temperature and dewpoint analyses, we evaluated data over a larger domain (330 × 330 km) than the wind analyses (150 × 150 km) to better distinguish the storm effects on the synoptic-scale thermodynamic fields.

Surface temperatures and dewpoints were composited over two 8 h periods to contrast the thermodynamic structure before and after landfall. The first period, from 0000 to 0800 GMT, was representative of the hurricane slowly strengthening until landfall. The second period, from 0800 to 1600 GMT, was representative of the storm weakening after landfall. These analyses are presented in Fig. 10. A lack of surface observations prevented analysis over water, but NOAA platform observations 40 km to the west of the storm indicated that sea surface temperatures were about 29°C and air temperatures were 25°–26°C, with lower temperatures (indicative of wet bulbing) in squalls. Surf temperatures at Galveston beach were 27°–28°C. Figure 10a indicates a pool of cool (24°C) air, just inland, and associated with outer rainband passage. Based on the sea surface temperatures mentioned earlier and studies that have indicated near-isothermal inflow at the surface in hurricanes over the open water (e.g., Byers, 1944) it was assumed that the surface air in the core of the storm was 26°–27°C (except in regions of strong oceanic mixing and upwelling; Black, 1983). Figure 10b shows that, after landfall, the surface temperatures over land in the core of the storm had decreased 2°–3°C. Local regions of cooler (23°C) air were found in areas traversed by the eyewall and outer intense rainbands.

Dewpoint temperatures before landfall in Fig. 10c show a northwest–southeast moisture gradient of 5°C over 100 km. Unfortunately, there were no surface dewpoint observations available over the water, but surface air in the core of the storm was probably near saturation so that temperatures were 25°–26°C. Figure 10d indicates that, after landfall, dewpoints in the core of the storm decreased 2°–3°C and dewpoints outside a 111 km radius of the center cooled 3°–4°C. With respect to land, the effect of the storm passage was to force dry air further from the coast, moistening the land where onshore flow had occurred and slightly drying the land in the offshore flow region.

Temperature analyses indicate that advection of cool air was not responsible for the cooling observed in the core region. Dewpoint analyses give some evidence of advection of drier air closer to the core of the storm on the north and west sides. The cooling and drying in the core of the storm was probably associated with loss of the surface sensible heat and moisture source. In the absence of surface heat fluxes, warm air would cool adiabatically while flowing in toward the center over land. In Alicia, the cooling did not appear to be concentrated in any one quadrant of the storm, whereas in Frederic (and in many U.S. landfalling storms as reported by Novlan and Gray, 1974) a cold air pool was noted in the front left quadrant where the longest over-land trajectories were located. Turbulent mixing of drier air from above the boundary layer, together with horizontal mixing of air from convective and mesoscale downdrafts, could further act to cool and dry the inflowing surface air.

The combined effect of the cooling and drying in the core of Alicia may be seen in the θ_e distribution. Figures 11a and 11b show flight-level calculations of θ_e (calculated according to Simpson's, 1978 method) for 8-h composites centered at prelandfall (0030 GMT) and landfall (0730 GMT). Direct surface measurements of quantities for the θ_e calculation were limited over land, but are shown in dashed lines where available. The θ_e values at flight level outside the core were about 5° lower than surface values in the same location with respect to the storm. By comparison, potential temperatures (not shown) at flight level were 6–7 K warmer than surface values. These data indicate that the lower levels were conditionally unstable. The 1500 m level is above the top of the boundary layer (where θ_e and θ are well mixed), but still well within the inflow layer as indicated by wind observations. An interesting feature of the θ_e analysis at landfall is the sharp boundary

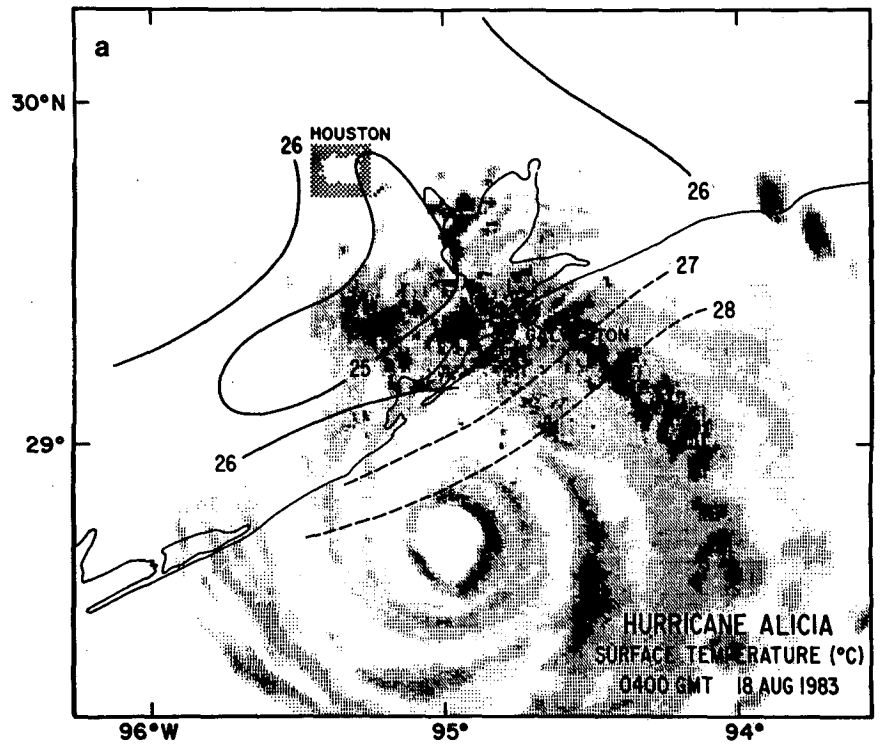

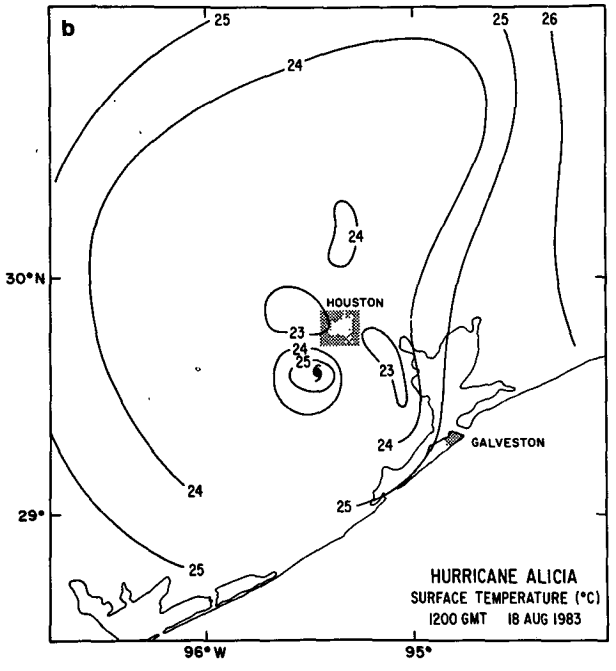

FIG. 10. Surface air temperature (in degrees Celsius) composite analyses for (a) 0000–0800 GMT, prelandfall, and (b) 0800–1600 GMT, postlandfall. Surface dewpoint temperature composites for (c) prelandfall and (d) postlandfall periods, as in (a) and (b). For Fig. 10a radar reflectivity is as in Fig. 3a, but for 0434 GMT, 18 August 1983.

between the core of >350 K air and the surrounding environment of 345 K air. As discussed in section 3a, this boundary formed at the axis of the outer rainband region in agreement with the stationary band complex theory of Willoughby et al. (1984).

It is important to recognize the time scale at which cooling and drying effects act to increase the surface pressure in the center of the storm. Figures 11a and 11b indicate that while the storm was proceeding from prelandfall to landfall, with the surface pressure dropping, the areal average θ_e in the core of the storm was decreasing in response to half of the circulation being over land. This is illustrated by the decreased area of $\theta_e > 350$ K. The numerical model landfall simulation

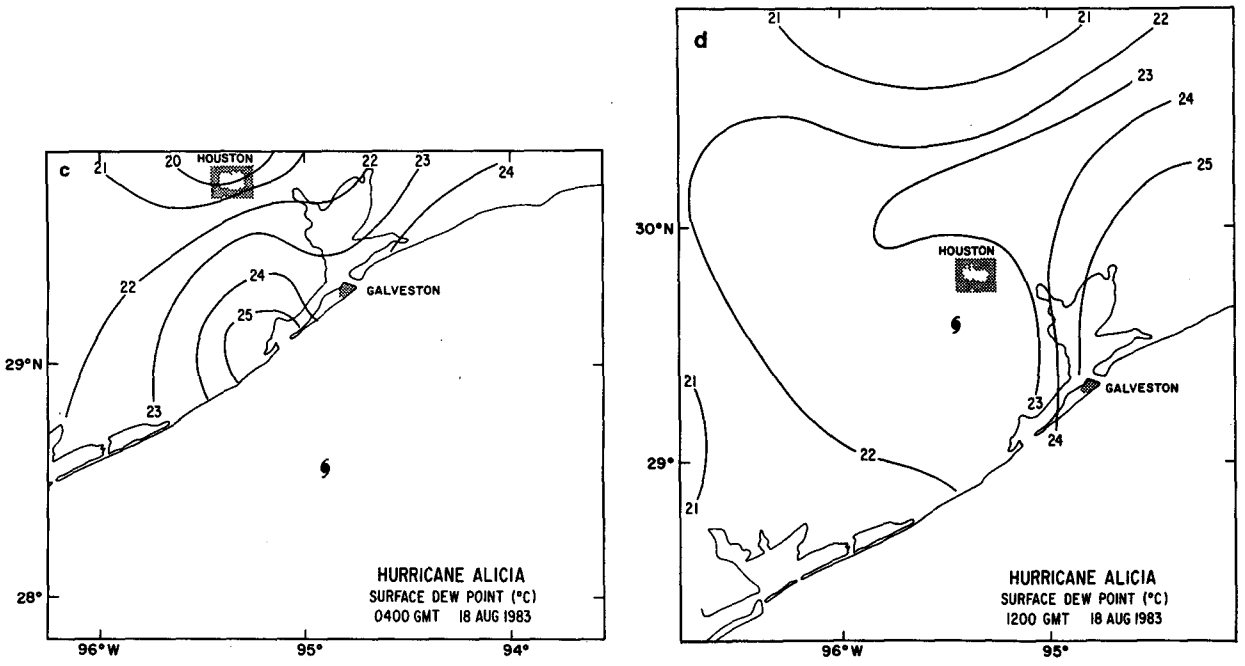

FIG. 10. (*Continued*)

of Tuleya et al. (1984) showed similar results with surface θ_e values 10°K lower over land than over the ocean and a decrease in the areal average of > 355°K θ_e over land. However, the maximum θ_e values near the center increased from 362 K at 0030 GMT to 365 K at 0730 GMT. While the storm was approaching landfall, the θ_e gradient increased and the sea level central pressure dropped even though the areal average θ_e decreased. Apparently, the upper levels were still being supplied high enough θ_e air, even though half of the storm's circulation was over land.

The temperature and dewpoint fields in Fig. 10 were combined with pressure observations to calculate the change in surface θ_e in the core of the storm from prelandfall (0400 GMT) to postlandfall (1200 GMT). Representative θ_e values at 30 km from the storm center (just outside the eyewall) indicate a decrease in θ_e from 364 to 353 K, which corresponded to a central pressure increase of 1.5 kPa (2.5 kPa increase to 1600 GMT). In Hurricane Frederic, a similar calculation yielded a decrease from 368 to 353 K over 8 h after landfall and associated with a central pressure increase of 3.3 kPa. Results from Alicia and Frederic show an average increase of 0.18 kPa per deg decrease of near-core surface θ_e, which compares well with the Malkus–Riehl relationship of 0.25 kPa per deg. This difference is probably due to dilute ascent (since the surface and flight level data indicate θ_e decreasing with height) of high surface θ_e in the core to middle levels rather than the near undilute ascent to upper levels implied by the Malkus–Riehl relationship.

4. Summary and discussion

Surface observations and NOAA aircraft measurements were used to document the wind and precipitation (radar reflectivity) fields in Hurricane Alicia as it approached and made landfall along the Texas coast.

Before landfall, Alicia displayed a symmetric, double eyewall structure with secondary wind maxima and weak inflow at flight level. At landfall, as observed in Hurricane Frederic, maximum surface winds occurred in the right front quadrant of the eyewall, and a strong land–sea asymmetry was apparent along the coastline where sustained winds over water were greater than over land. This produced convergence in the onshore flow at the coast. At landfall, the concentric eyewall structure started to lose its organization over land, but was still apparent over water. As the outer rainband axis (defined by a secondary wind maximum and a sharp θ_e change at flight level) passed the northeast end of Galveston Island, surface wind observations indicated strong confluence toward the band axis. Most of the tornadoes reported during Alicia formed inland in this outer rainband region in agreement with the studies of Novlan and Gray (1974) and Gentry (1984).

The rainband axis was associated with strong surface convergence while the area between the axis and the eyewall displayed surface divergence. Although not evident in the prelandfall observations, it appears that at landfall, the outer band axis to the northeast of the storm acted as an obstruction to the surface flow. The rainband represented a boundary delineating the tran-

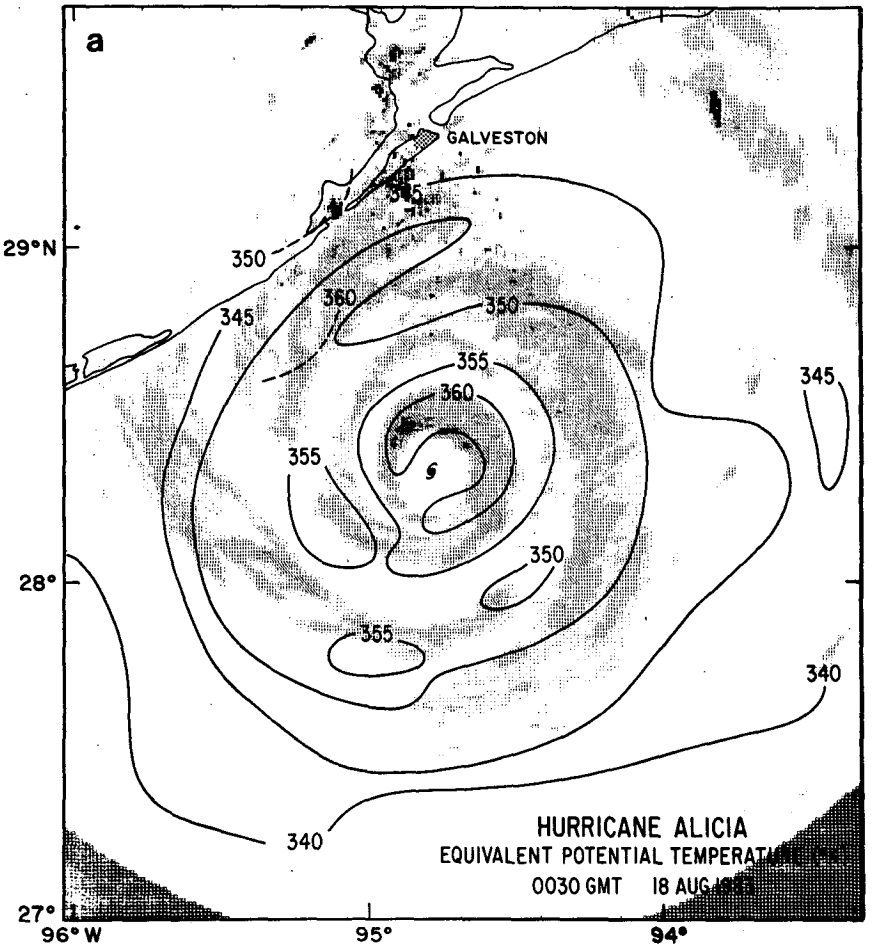

FIG. 11. Flight-level composites of equivalent potential temperature (in deg K) for (a) 0030 GMT prelandfall center time, and (b) 0730 GMT landfall center time. (Surface values are indicated by dashed lines.)

sition region between the core of the storm and the environment through which the storm moved, in agreement with the stationary-band complex theory of Willoughby et al. (1984). This effect was only weakly present at flight level, however, in contrast to the study of the Hurricane Floyd rainband by Barnes et al. (1983).

The Hurricane Frederic landfall study and numerical model simulations suggest that, in general, divergence and a rainfall minimum should occur on the left side of a landfalling storm where the flow accelerates off the land. In Alicia, however, surface convergence, an increase in radar reflectivity, and a maximum in inflow angle were observed where offshore flow met with flow paralleling the coastline over water. Again, as on the northeast side of the storm near Galveston, these features were not evident at flight level. The inflow maximum on the left side of the storm was apparently related to asymmetries produced by the southwest–northeast coastline orientation and an environmental flow from the southwest. These characteristics would tend to reinforce inflow on the southwest side of the storm and reduce inflow on the northeast side.

An analysis of the total asymmetric surface flow field at landfall indicated that asymmetric components of the flow could be attributed to the land–sea roughness difference and coastline orientation, the storm translation velocity, and the southwest environmental flow. These components may interact with the vortex circulation to produce asymmetrical convergence fields that are related to the distribution of convection. The success of the slab boundary-layer model of Shapiro (1983) in producing convergence distributions that compared well with radar reflectivity patterns in open ocean hurricanes suggests that further modeling studies be undertaken to determine the importance of the land–sea asymmetry and the coastline orientation in determining the distribution of convergence.

Alicia weakened slowly after landfall and maintained sustained hurricane force winds in the eyewall for at least 6 h. These winds were responsible for much of

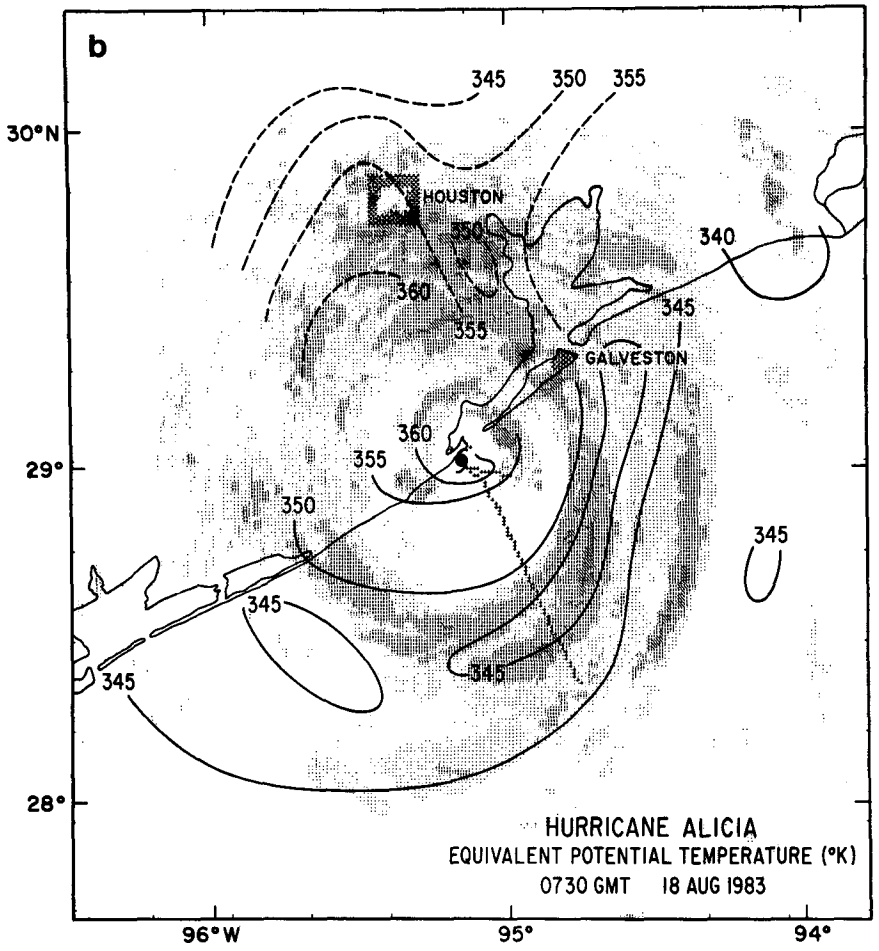

FIG. 11. (*Continued*)

the damage in the downtown Houston area. The rapid sea-level pressure increase after landfall was a hydrostatic adjustment produced by a decrease in surface θ_e leading to reductions in the upper-level convective heat source and compensating subsidence. The surface θ_e decrease was most likely produced by the absence of a surface moisture and heat source.

An important finding of this study is the observation that, at landfall, features that are strongly present at the surface within the boundary layer may be absent, or only weakly present, at flight level. It is apparent, from the sharp vertical and horizontal discontinuities in the wind field, that the hurricane boundary layer may respond to landfall through readjustments on a scale of several hours. This reaction may be related to the dynamics of principal rainbands.

This finding illustrates the problems that can occur when reconnaissance observations are used for guidance when forecasting surface conditions and preparing warnings for landfalling hurricanes. In landfalling storms, safety requirements prevent aircraft from overflying land and often force the aircraft to fly at altitudes well above the top of the hurricane boundary layer. The only remedy for these problems is to improve the remote sensing capabilities of reconnaissance aircraft to provide near real-time measurements of wind velocity at the surface and other levels below the aircraft. Recent additions of the airborne Doppler radar and a stepped-frequency microwave radiometer, in addition to future microwave scatterometer systems (Jones et al., 1981), hold much promise for deducing the flow within the hurricane boundary layer.

Acknowledgments. The author would like to thank several individuals for their cooperation and dedication in obtaining meteorological observations for poststorm analyses during a time of stress following landfall. Such data are extremely important in gaining an understanding of the dynamics of landfalling hurricanes and ultimately improving our ability to forecast the behavior of these destructive storms. Among those who contributed to this research are the Galveston National Weather Service Office personnel under the direction of Bill Blum, Bryan Lambeth of Radian Corporation,

Chief Martin of the U.S. Coast Guard Group, Galveston, Dr. Richard Marshall of the National Bureau of Standards, George Huebner of Texas A&M University, Tim Marshall of Haag Engineering, Joe Muscanere of SWS Communications, Jimmie O'Donnell of Braes Meadow, Kenneth Hill of Exxon, weather enthusiasts Barbara White and Al Wooten, and the personnel of the NOAA Office of Aircraft Operations (OAO). Special thanks goes to the Hurricane Research Division land-based radar team of Frank Marks and Allen Farr, and to Phil Bogert, OAO, for most of the database creation. The paper benefited from several helpful discussions with Drs. Peter Black and Stephen Lord of the Hurricane Research Division. The figures were drafted by Dale Martin and Sue O'Brien of the AOML Graphics Department.

APPENDIX

Applications to Hurricane Surface Wind Forecasting

Flight-level wind, pressure, and temperature information are available to hurricane forecasters from NOAA reconnaissance (recon) aircraft before landfall via an aircraft-satellite data link (ASDL). Forecasters may use this information as guidance in the preparation of warnings and forecasts of surface wind conditions, damage potential, and storm surge at landfall.

Recon observations include half-hourly ASDL bursts of filtered meteorological data reported each minute (see Pifer et al., 1978, and Parrish et al., 1984, for further information on the ASDL system). The 1 s aircraft observations are input continuously to a first-order autoregressive filter (FOAR; Merceret, 1983) and sampled each minute. The FOAR filter has a half-power period of 60 s, meaning that velocity fluctuations with time scales of <60 s are smoothed with variance reduced by more than 50%. Therefore, the filter smoothes out turbulent and convective-scale fluctuations and allows "real-time" sampling. In addition to the 1 min information, ASDL transmissions may also contain the vortex message, which includes determination of the maximum flight-level wind and the surface wind when the sea surface is visible. As an aid in assimilating these data, it is important to compare these quantities to averages made from the 1 s flight-level observations and to surface wind measurements. Such a comparison is presented in Table 1 for five recon storm center fixes before landfall. As shown in Table 1, the 1 min sampled ASDL wind speeds are about 5% less than 30 s and 60 s averages made near the same time. The maximum wind as reported in the vortex message compared well

TABLE 1. Comparison of reconnaissance maximum wind speed reports with flight-level (1500 m) averaged winds and maximum surface winds at landfall.

Fix time (GMT)	Minimum pressure (mb)	Maximum ASDL wind ($m\ s^{-1}$) (GMT)	Maximum 30-s mean flight level wind ($m\ s^{-1}$) (GMT)	Maximum 60-s mean flight level wind ($m\ s^{-1}$)	Estimate of surface wind from flight level (vortex message) range and bearing from eye	Maximum 10 m (model-computed) mean wind ($m\ s^{-1}$)	Maximum flight level wind ($m\ s^{-1}$) (vortex message) range (km) and bearing from eye	Maximum 2 s flight level wind ($m\ s^{-1}$)
17 August		(2058)	(2058)				165°	
2102	973	151° 43.8	147° 46.5	46.5	33.5 56 km E	34.1	56 km E 43.8	47.7
18 August		(0200)	(0200)				150°	
0012	968	289° 41.7	300° 45.9	45.0	N/A	33.9	46 km NE 46.4	46.9
		(0256)	(0256)				165°	
0259	966	171° 42.8	172° 44.2	43.5	N/A	32.7	28 km E 46.4	44.2
		(0622)	(0622)				230°	
0625	963	220° 44.3	223° 47.8	46.0	N/A	35.0	28 km SE 48.8	49.9
		*(0736)	(0737)				155°	
0643	962	139° 50.1	152° 46.3	46.0	N/A	33.9	56 km ENE 46.4	46.5
		(0737)						
		153° 42.3						

Maximum coastal mean winds ($m\ s^{-1}$)				
	0700 Z	BWD	39	Gust to 48
		GLS	19	Gust to 40
	1100 Z	USI	26	Gust to 35
		CLP	25	Gust to 46
Peak gust	0750 Z	BWD	55.4	

Key: BWD—USCG Cutter *Buttonwood;* GLS—Galveston Weather Service Office; USI—U.S. Industrial Chemical Co., Houston; CLP—USCG *Clamp.* * 0736 GMT ASDL OB contaminated by 2 s differential pressure error.

TABLE 2. Ratios of the 10 m level over-water wind (V_o), over-land wind (V_L), and over-land peak gust (V_{LG}) to the flight-level (1500 m) wind (V_a).

Aircraft time (GMT)	Land station time (GMT) Relative position from storm center	V_o 30 s 10 m mean (model-computed) (m s^{-1})	V_a 30 s mean wind (m s^{-1})	V_L 10-m mean land (m s^{-1})	V_{LG} 10-m land gust	V_o/V_a	V_L/V_o	V_L/V_a	V_{LG}/V_a	Gust factor $G = V_{LG}/V_L$
0628	DOA 0655 22 km SW	24.1	30.8	22.4	28.6	0.78	0.93	0.73	0.93	1.3
0629	DOB 0735 22 km SW	22.6	28.6	24.3	41.4	0.79	1.07	0.85	1.44	1.8
0651	PSX 1100 130 km SW	14.7	17.6	11.0	15.6	0.83	0.75	0.63	0.89	1.42
0734	GLS 0920 40 km NE	27.8	36.4	19.2	39.2	0.76	0.69	0.53	1.1	2.1
0735	GLS 0900 44 km NE	28.3	37.1	17.4	37.3	0.76	0.61	0.47	1.00	2.2
0748	BPT 1000 154 km NE	24.2	30.7	12.3	21.1	0.78	0.51	0.40	0.69	1.75
0750	BPT 1100 155 km NE	26.2	33.6	13.4	22.6	0.78	0.51	0.40	0.67	1.7
0846	DOA 0855 34 km SSW	26.5	36.5	18.3	29.1	0.72	0.69	0.50	0.80	1.6
0847	DOA 0925 38 km SSW	25.3	32.4	21.5	31.7	0.78	0.85	0.66	0.98	1.4
0848	DOB 0955 45 km SSW	23.6	30.1	19.2	27.3	0.78	0.81	0.64	0.91	1.4
0849	DOA 0955 45 km SSW	24.5	31.4	23.7	37.1	0.78	0.97	0.75	1.18	1.5
0849	DOB 1025 55 km SSW	24.5	31.4	17.9	29.5	0.78	0.73	0.57	0.94	1.6
0850	DOB 1055 55 km SSW	24.5	31.4	16.6	26.0	0.78	0.68	0.53	0.83	1.5
Mean:						0.78	0.75	0.59	0.95	1.64
Standard Deviation:						0.02	0.17	0.14	0.21	0.27

with the 2 s mean and the only available estimate of the surface wind compared well with an estimate from the diagnostic boundary layer model (Powell, 1980). All ASDL and vortex message winds were larger than the maximum sustained inland and coastal surface (10 m) winds measured during the storm. However, the peak surface gust of 55 m s^{-1} observed by the USCG vessel *Buttonwood* was larger than any of the reported maximum flight-level winds. This gust was associated with the passage of the outer rainband shown in the vicinity of Galveston in Fig. 4a and occurred just after the aircraft had sampled the region.

To assist forecasters in estimating surface wind conditions at landfall using recon data as guidance, relationships were developed between aircraft flight-level wind speeds, surface coastal observations over land and over water, and surface wind estimates from a diagnostic PBL model (Powell, 1980). Comparisons of aircraft and surface land station wind measurements (Table 2) were possible when data from the landfall composite analysis time period were plotted in the same relative location (within 10 km) with respect to the storm center. Similar comparisons were made in a study of Hurricane Frederic by Powell (1982). Table 2, with Frederic results in parentheses, indicates that the 10-m level PBL model-computed, over-water mean wind, V_o, was 78% (71%) of the flight-level (30 s) mean wind, V_a; the surface (10 m) over-land mean wind, V_L, was 75% (81%) of V_o, and 59% (58%) of V_a; the surface (10 m) over-land wind gust, V_{LG}, was 95% (80%) of V_a; and 1.6 (1.4) was a typical gust factor for the land stations.

The data in Table 2 displayed a variability that depended upon the time and space differences between aircraft and surface observations, the proximity of convective rainbands and the exposure of the site as shown by the large standard deviations in Table 1. Comparison with the Hurricane Frederic values indicates that these percentages may vary from storm to storm. The wind relationships may be inaccurate near rainbands during landfall, as shown by the large differences between surface winds and flight-level observations on the northeast side of Alicia. It should again be noted that the representativeness of aircraft measurements for use in forecasting surface effects depends upon the altitude of the aircraft. The estimates in Table 2 should only be used when an aircraft is within or just above the boundary layer, i.e., <1500 m. These percentages may be used with ASDL flight-level wind speeds, by adjusting the ASDL wind upward by 5%.

REFERENCES

Anthes, R. A., 1982: *Tropical Cyclones, Their Evolution, Structure and Effects. Meteor. Monogr.*, No. 41, Amer. Meteor. Soc., 208 pp.

Barnes, G. M., E. J. Zipser, D. P. Jorgensen and F. D. Marks, Jr., 1983: Mesoscale and convective-scale structure of a hurricane rainband. *J. Atmos. Sci.*, **40**, 2125–2137.

Black, P. G., 1983: Ocean temperature changes induced by tropical cyclones. Ph.D. dissertation, The Pennsylvania State University, 278 pp.

——, and W. L. Adams, 1983: Guidance for estimating surface winds based on sea state observations from aircraft and sea state catalog. Fed. Coord. for Meteor. Serv. and Supporting Res., FCM-G1-1983, U.S. Dept. Commerce, NOAA, Washington, DC, 84 pp.

Byers, H. R., 1944: *General Meteorology.* McGraw Hill, 645 pp.

Case, R. A., and H. P. Gerish, 1984: Atlantic hurricane season of 1983. *Mon. Wea. Rev.*, **112**, 1083–1092.

Chow, S., 1971: A study of the wind field in the planetary boundary layer of a moving tropical cyclone. M.S. thesis, Dept. of Meteor. Ocean., New York University, 59 pp. [Available from Library, AOML, 4301 Rickenbacker Causeway, Miami, Florida 33149.]

Durst, C. S., 1960: Wind speeds over short periods of time. *Meteor. Mag.*, **89**, 181–186.

Fujita, T. T., 1979: Damage map of Hurricane Frederic, September 12–13, 1979, University of Chicago. [Available from AOML/HRD, 4301 Rickenbacker Causeway, Miami, Florida 33149.]

Gentry, R. C., 1983: Genesis of tornadoes associated with hurricanes. *Mon. Wea. Rev.*, **111**, 1793–1805.

Jones, W. L., P. G. Black, V. E. Delnore and C. L. Swift, 1981: Airborne microwave remote sensing measurements of Hurricane Allen. *Science*, **214**, 274–280.

Jorgensen, D. P., 1984: Mesoscale and convective-scale characteristics of mature hurricanes. II: Inner core structure of Hurricane Allen (1980). *J. Atmos. Sci.*, **41**, 1287–1311.

Krishnamurti, T. N., 1962: Some numerical calculations of the vertical velocity field in hurricanes. *Tellus*, **14**, 195–211.

Lamberth, B., 1983: Hurricane Alicia: Special report. DCN 83-120-280-38, Radian Corporation, Austin.

Malkus, J. S., and H. Riehl, 1960: On the dynamics and energy transformations in steady-state hurricanes. *Tellus*, **12**, 1–20.

Marks, F. D., Jr., and R. A. Houze, 1984: Airborne Doppler radar observations in Hurricane Alicia. *Proc. 22nd Conf. on Radar Meteorology*, Zurich, Amer. Meteor. Soc., 578–583.

Marshall, R. D., 1984: Fastest-mile wind speeds in Hurricane Alicia. NBS Tech. Note 1197, U.S. Dept. Commerce, Natl. Bur. Stand., Washington, DC.

Merceret, F. J., 1983: First-order autoregressive low-pass filters: A quick reference handbook. NOAA Tech. Memo. ERL RFC-9, NOAA, Office of Aircraft Operations, Miami, Florida.

——, and H. Davis, 1981: The determination of navigational and meteorological variables measured by NOAA/RFC WP-3D aircraft. NOAA Tech. Memo. ERL RFC-7, NOAA, Office of Aircraft Operations, Miami, FL.

Miller, B. I., 1964: A study on the filling of Hurricane Donna (1960) over land. *Mon. Wea. Rev.*, **92**, 389–406.

Moss, M. S., and R. W. Jones, 1978: A numerical simulation of hurricane landfall. NOAA Tech. Memo. ERL NHEML-3, U.S. Dept. Commerce, 15 pp. [available from AOML/HRD, 4301 Rickenbacker Causeway, Miami, FL 33149.]

Myers, V. A., and W. Malkin, 1961: Some properties of hurricane wind fields as deduced from trajectories. NHRP Rep. 49, 45 pp. [AOML/HRD, 4301 Rickenbacker Causeway, Miami, FL 33149.]

Novlan, D. J., and W. M. Gray, 1974: Hurricane-spawned tornadoes. *Mon. Wea. Rev.*, **102**, 476–488.

Panofsky, H. A., and J. A. Dutton, 1984: *Atmospheric Turbulence.* Wiley Interscience, 397 pp.

Parrish, J. R., R. W. Burpee, F. D. Marks and R. Grebe, 1982: Rainfall patterns observed by digitized radar during the landfall of Hurricane Frederic (1979). *Mon. Wea. Rev.*, **110**, 1933–1944.

——, R. W. Burpee, F. D. Marks, Jr. and C. W. Landsea, 1984: Mesoscale and convective-scale characteristics of Hurricane Frederic during landfall. *Proc. 15th Conf. on Hurricanes and Tropical Meteorology*, Miami, Amer. Meteor. Soc., 415–420.

——, E. R. Darby, J. D. DuGranrut and A. S. Goldstein, 1984: The NOAA aircraft satellite data link (ASDL). NOAA Tech. Memo. OAO-3, NOAA, Office of Aircraft Operations, Miami, FL, 35 pp.

Pifer, B., M. Zimmer, J. DuGranrut and J. McFadden, 1978: Aircraft–satellite data link. *Bull. Amer. Meteor. Soc.*, **59**, 288–290.

Powell, M. D., 1980: Evaluations of diagnostic marine boundary layer models applied to hurricanes. *Mon. Wea. Rev.*, **108**, 757–766.

——, 1982: The transition of the Hurricane Frederic boundary layer wind fields from the open Gulf of Mexico to landfall. *Mon. Wea. Rev.*, **110**, 1912–1932.

——, and P. G. Black, 1984: Airborne Doppler radar observations

of the boundary layer of Hurricane Debby (1982). *Proc., 22nd Conf. on Radar Meteorology,* Zurich, Amer. Meteor. Soc., 584–588.

——, F. D. Marks, Jr. and P. G. Black, 1984: The asymmetric structure of Alicia's wind field at landfall. ASCE Specialty Conference, "Hurricane Alicia, One Year Later," ASCE Press, N.Y.

Rosenthal, S. L., 1971: The response of a tropical cyclone model to variations in boundary layer parameters, initial conditions, lateral boundary conditions, and domain size. *Mon. Wea. Rev.*, **99,** 767–777.

Savage, R. P., J. Baker, J. H. Golden, A. Kareem and B. R. Manning, 1984: Hurricane Alicia, Galveston and Houston, Texas, August 17–18, 1983. Comm. on Natural Disasters, National Research Council, National Academy Press, Washington, DC, 158 pp.

Shapiro, L. J., 1983: The asymmetric boundary layer flow under a translating hurricane. *J. Atmos. Sci.*, **40,** 1984–1998.

——, and H. E. Willoughby, 1982: The response of balanced hurricanes to local sources of heat and momentum. *J. Atmos. Sci.*, **39,** 378–394.

Sherman, L., 1956: On the wind asymmetry of hurricanes. *J. Meteor.*, **13,** 501–503.

Simpson, R. H., 1978: On the computation of equivalent potential temperature. *Mon. Wea. Rev.*, **106,** 124–130.

Steigler, D. J., 1983: Damage map of Hurricane Alicia, August 17–18, 1983, University of Chicago. (Available from AOML/HRD, 4301 Rickenbacker Causeway, Miami, FL 33149.)

Storm Data, 1983: Outstanding storms of the month, 25(8) National Climatological Data Center, NESDIS, NOAA, Federal Bldg., Asheville, NC, 28801.

Tuleya, R. E., and Y. Kurihara, 1978: A numerical simulation of the landfall of tropical cyclones. *J. Atmos. Sci.*, **35,** 242–257.

——, M. A. Bender and Y. Kurihara, 1984: A simulation of the landfall of tropical cyclones using a moveable nested-mesh model. *Mon. Wea. Rev.*, **112,** 124–136.

Willoughby, H. E., 1985: Confirmatory observations of concentric eyes in hurricanes. *Ex. Abst., 16th Conf. on Hurricanes and Tropical Meteorology,* Houston, Amer. Meteor. Soc., 1–2.

——, J. A. Clos and M. G. Shoreibah, 1981: Concentric eye walls, secondary wind maxima, and the evolution of the hurricane vortex. *J. Atmos. Sci.*, **39,** 395–411.

——, F. D. Marks, Jr. and R. J. Feinberg, 1984: Stationary and propagating convective bands in asymmetric hurricanes. *J. Atmos. Sci.*, **41,** 3189–3211.